Chemical Engineering Journal 446 (2022) 137300

Contents lists available at ScienceDirect

Chemical Engineering Journal

journal homepage: www.elsevier.com/locate/cej

Polyvinylidene fluoride membrane formation using carbon dioxide as a non-solvent additive for nuclear wastewater decontamination

Mohamed Essalhi [a], Norafiqah Ismail [a], Solomon Tesfalidet [a], Jun Pan [b], Qian Wang [b], Zhoaliang Cui [b,*], M.C. García-Payo [c], Mohamed Khayet [c,d], Jyri-Pekka Mikkola [a,e], Shokat Sarmad [a], Denis Bouyer [f], Yun Zhao [g], Baohua Li [g], C. André Ohlin [a], Naser Tavajohi [a,*]

[a] Department of Chemistry, Umeå University, 90187 Umeå, Sweden
[b] State Key Laboratory of Materials-Oriented Chemical Engineering, College of Chemical Engineering, Nanjing Tech University, Nanjing 211816, China
[c] Department of Structure of Matter, Thermal Physics and Electronics, Faculty of Physics, University Complutense of Madrid, Avda. Complutense s/n, 28040 Madrid, Spain
[d] Madrid Institute for Advanced Studies of Water (IMDEA Water Institute), Calle Punto Net N° 4, 28805, Alcalá de Henares, Madrid, Spain
[e] Industrial Chemistry & Reaction Engineering, Johan Gadolin Process Chemistry Centre, Åbo Akademi University, Biskopsgatan 8, 20500 Åbo-Turku, Finland
[f] Institut Européen des Membranes, IEM, UMR 5635, ENSCM, CNRS, Univ Montpellier, Montpellier, France
[g] Shenzhen Key Laboratory on Power Battery Safety and Shenzhen Geim Graphene Center, Tsinghua Shenzhen International Graduate School (SIGS), Shenzhen 518055, China

ARTICLE INFO

Keywords:
Carbonated coagulation bath
Ternary phase diagram
Membrane distillation
Simulated nuclear wastewater treatment
Nuclides decontamination
Desalination

ABSTRACT

Polyvinylidene fluoride (PVDF) membranes were prepared by phase inversion in the most commonly used solvents for membrane manufacture, with CO_2 as a non-solvent additive. The effects of changing the polymer concentration (10, 12.5 and 15% by weight), the type of solvent (NMP, DMAc and DMF) and the coagulation bath with three levels of CO_2 concentration on the phase inversion process, as well as the phase diagram, morphology and transport properties of the membranes were studied. The best performing membranes were used to desalinate salt aqueous solutions and decontaminated simulated nuclear wastewater by membrane distillation using two configurations (DCMD and AGMD). All selected membranes showed high rejection with acceptable permeate fluxes reaching an infinite decontamination factor. The proposed approach of this novel idea of using CO_2 dissolved in water as a coagulation medium in the field of membranes avoids the increase of the harmful effect on the environment caused by the addition of a harsh non-solvent to the coagulation bath. It constitutes a beneficial use of carbon dioxide that reduces the negative environmental impact of membrane manufacturing and represents a decisive step towards its sustainability. Furthermore, this study highlights the potential benefits of using these membranes in DM for desalination and treatment of simulated nuclear wastewater.

Abbreviations: AGMD, Air gap membrane distillation; DCMD, Direct contact membrane distillation, *DF*, Decontamination factor; DMAC, *N*, *N*-dimethylacetamide; DMF, Dimethylformamide; EDX, Energy dispersive X-ray spectroscopy; FESEM, Field emission scanning electron microscope; FTIR, Fourier transform infrared spectroscopy; ICP-OES, Inductively coupled plasma optical emission spectrometer; IPA, Isopropyl alcohol; LCP, Linearized cloud point; LEP_w, Water entry pressure (10^5 Pa); MD, Membrane Distillation; NMP, 1-methyl-2-pyrrolidinone; NIPS, Non-solvent phase inversion; PVDF, Polyvinylidene fluoride; PWP, Pure water permeability ($kg.m^{-2}.h^{-1}.bar^{-1}$); SNWW, Salty simulated nuclear wastewater; C_0, Initial salt concentration in the permeate (g/L); C_1, Final salt concentration in the permeate (g/L); $C_{f,\,i}$, Measured concentration of nuclides (i) in the feed solution (ppm); $C_{p,\,i}$, Measured concentration of nuclides (i) in the permeate solution (ppm); $D_{A\text{-}B}$, Diffusion coefficient of solute A in solvent B ($cm^2{\cdot}s^{-1}$); J_p, Permeate flux ($kg{\cdot}m^{-2}{\cdot}h^{-1}$); M_w, Molecular weights ($g{\cdot}mol^{-1}$); n_{CO2}, Number of moles of dissolved CO_2 in the solvent; $T_{f,\,in}$, Feed inlet temperature (°C); $T_{p,\,in}$, Permeate inlet temperature (°C); W, Weight (g); α, Salt rejection factor (%); δ_i, Solubility parameter of component i; ε, Porosity (%); ρ, Density ($g{\cdot}cm^{-3}$); ϕ_i, Weight fraction of component (i); χ_{CO2}, mole fraction of CO_2 in a given solvent; Ω_p, Permeate electrical conductivity (μS/cm); $\Omega_{p,\,f}$, Final permeate electrical conductivity (μS/cm); $\Omega_{p,\,i}$, Initial permeate electrical conductivity (μS/cm).

* Corresponding authors.
E-mail addresses: zcui@njtech.edu.cn (Z. Cui), naser.tavajohi@umu.se (N. Tavajohi).

https://doi.org/10.1016/j.cej.2022.137300
Received 14 February 2022; Received in revised form 3 May 2022; Accepted 28 May 2022
Available online 31 May 2022

Table 1
Organic solvents and nonsolvents commonly used in the fabrication of phase inversion membranes.

Nonsolvent additive[a]	Polymer	Solvent[a]	Nonsolvent[a]	Effect in membrane formation	Ref
IPA	PVDF-HFP (Solef 21510)	TEP	H_2O	Delayed liquid–liquid phase demixing	[5]
MeOH	PVDF-HFP (Solef 21510)	TEP	H_2O	Delayed liquid–liquid phase demixing	[5]
TEP	PVDF-HFP (Solef 21510)	TEP	H_2O	Delayed liquid–liquid phase demixing	[5]
—	Cellulose (α-cellulose ~ 94 wt%)	NMMO	H_2O	Instantaneous liquid–liquid phase demixing	[6]
—	Cellulose (α-cellulose ~ 94 wt%)	(NMMO	i-BuOH	Delayed liquid–liquid phase demixing	[6]
MeOH	PVDF (Kynar HSV 900)	NMP	H_2O	Delayed liquid–liquid phase demixing	[7]
EtOH	PVDF (Kynar HSV 900)	NMP	H_2O	Delayed liquid–liquid phase demixing	[7]
i-PrOH	PVDF (Kynar HSV 900)	NMP	H_2O	Delayed liquid–liquid phase demixing	[7]
MeOH	PVDF (FR904)	DMAc	H_2O	Delayed liquid–liquid phase demixing	[8]
EtOH	PVDF (FR904)	DMAc	H_2O	Delayed liquid–liquid phase demixing	[8]
i-PrOH	PVDF (FR904)	DMAc	H_2O	Delayed liquid–liquid phase demixing	[8]
——	PVDF (250–450 K)	NMP	H_2O	Instantaneous liquid–liquid phase demixing	[9]
——	PVDF (250–450 K)	NMP	MeOH	Delayed liquid–liquid phase demixing	[9]
—	PVDF (Solef 6010)	DMAc	Water	Instantaneous liquid–liquid phase demixing	[10]
—	PVDF (Solef 6010)	DMAc	MeOH	Crystallization before delayed liquid–liquid phase demixing	[10]
—	PVDF (Solef 6010)	DMAc	t-BuOH	Crystallization before delayed liquid–liquid phase demixing	[10]
—	PVDF (Solef 6010)	DMAc	t-BuOH	Crystallization before delayed liquid–liquid phase demixing	[10]
—	PVDF (Solef 6010)	DMAc	1-Hexanol	Crystallization before delayed liquid–liquid phase demixing	[10]
—	PVDF (Solef 6010)	DMAc	1-Octanol	Crystallization before delayed liquid–liquid phase demixing	[10]
—	PBI	DMAc	Hexane	Instantaneous liquid–liquid phase demixing	[11]
—	PBI	DMAc	Xylene	Instantaneous liquid–liquid phase demixing	[11]
—	PBI	DMAc	Acetone	Delayed liquid–liquid phase demixing	[11]
—	PBI	DMAc	EA	Delayed liquid–liquid phase demixing	[11]
—	PBI	DMAc	BA	Delayed liquid–liquid phase demixing	[11]
—	PBI	DMAc	H_2O	Instantaneous liquid–liquid phase demixing	[11]
—	PBI	DMAc	MeOH	Delayed liquid–liquid phase demixing	[11]
—	PBI	DMAc	EtOH	Delayed liquid–liquid phase demixing	[11]
—	PBI	DMAc	IPA	Delayed liquid–liquid phase demixing	[11]
—	PBI	DMAc	IBA	Delayed liquid–liquid phase demixing	[11]
IPA	PVDF (HSV 900)	TEP	H_2O	Delayed liquid–liquid phase demixing	[12]
TEP	PVDF (HSV 900)	TEP	H_2O	Delayed liquid–liquid phase demixing	[12]
IPA	PVDF (M_W: 180, 275, and 533 kDa)	TEP	H_2O	Crystallization occurs prior to liquid–liquid demixing	[13]
——	PVDF (Kynar 740)	DMF	H_2O	Instantaneous liquid–liquid phase demixing	[14]
——	PVDF (Kynar 740)	DMF	1-octanol	Crystallization occurs prior to liquid–liquid demixing	[14]
NMP	PPSU (51 kD)	NMP	H_2O	Delayed liquid–liquid phase demixing	[15]
NMP/EtOH	PPSU (51 kD)	NMP	H_2O	Delayed liquid–liquid phase demixing	[15]
——	Extem	NMP	MeOH	Instantaneous liquid–liquid phase demixing	[16]
——	Extem	NMP	Glycerol	Delayed liquid–liquid phase demixing	[16]
DMAc	6FDA–4,4′ODA polyimide	NMP	H_2O	Delayed liquid–liquid phase demixing	[17]
AA-$NaHCO_3$	Radel S-PPSU (R-5000)	NMP	IPOH	Delayed liquid–liquid phase demixing	[18]
NMP	PSF Udel P-3500	NMP	H_2O	Delayed liquid–liquid phase demixing	[19]
DMSO	EVAL (105A)	DMSO	H_2O	Delayed liquid–liquid phase demixing	[20]
———	PVDF (Kynar 760)	NMP	H_2O	Instantaneous liquid–liquid phase demixing	[21]
———	PVDF (Kynar 760)	NMP	Pr-OH	Delayed liquid–liquid phase demixing	[21]
Acetone	CA (50 kDa)	NMP	H_2O	Delayed liquid–liquid phase demixing	[22]

(*continued on next page*)

Table 1 (*continued*)

Nonsolvent additive[a]	Polymer	Solvent[a]	Nonsolvent[a]	Effect in membrane formation	Ref
———	PVDF (Kynar 961)	DMF	1-octanol	Crystallization occurs prior to liquid–liquid demixing	[23]
———	Terpolymer (Kynar 9301)	DMF	1-octanol	Crystallization occurs prior to liquid–liquid demixing	[23]
———	PVDF (Solef 1015)	TEP and DMAc	H_2O	Instantaneous liquid–liquid phase demixing	[24]
———	PVDF (Solef 1015)	TEP and DMAc	EtOH	Delayed liquid–liquid phase demixing	[24]
EtOH	PVDF (Solef 6020)	DMF	H_2O	Delayed liquid–liquid phase demixing	[25]
———	PVDF (Solef 6020)	DMF	H_2O	Instantaneous liquid–liquid demixing	[25]
Rhodiasolv PolarClean	PVDF (Solef 1015)	Rhodiasolv PolarClean	H_2O	Delayed liquid–liquid phase demixing	[26]
———	PC (*Mw*: 33 K)	DMAc	EtOH	Delayed liquid–liquid phase demixing	[27]
———	PC (*Mw*: 33 K)	DMAc	PrOH	Delayed liquid–liquid phase demixing	[27]
———	PC (*Mw*: 33 K)	DMAc	BuOH	Delayed liquid–liquid phase demixing	[27]
———	PC (*Mw*: 33 K)	DCM	EtOH	Delayed liquid–liquid phase demixing	[27]
———	PC (*Mw*: 33 K)	DCM	PrOH	Delayed liquid–liquid phase demixing	[27]
———	PC (*Mw*: 33 K)	DCM	BuOH	Delayed liquid–liquid phase demixing	[27]
———	PVDF (Hylar 5000)	TEP	H_2O	Instantaneous liquid–liquid phase demixing	[28]
TEP	PVDF (Hylar 5000)	TEP	H_2O	Delayed liquid–liquid phase demixing	[28]
NaOH	PAN	NMP	H_2O	Delayed liquid–liquid phase demixing	[29]
DMAc	PI	DMAc	EtOH	Delayed liquid–liquid phase demixing	[30]
Na_2SO_4/KOH	PVA	Water	H_2O	Delayed liquid–liquid phase demixing	[31]
————	PVDF/ CA	DMAc	H_2O	Instantaneous liquid–liquid phase demixing	[32]
EtOH	PVDF/CA	DMAc	H_2O	Crystallization occurs prior to liquid–liquid demixing	[32]
———	PVDF (Solef 1015)	NMP	H_2O	Instantaneous liquid–liquid phase demixing	[33]
NMP	PVDF (Solef 1015)	NMP	H_2O	Delayed liquid–liquid phase demixing	[33]
Glycerol	PVDF (Solef 1015)	NMP	H_2O	Delayed liquid–liquid phase demixing	[33]
DMF	PU (Estane 5701Fl)	DMF	H_2O	Delayed liquid–liquid phase demixing	[34]
———	PVDF (Kynar 740)/PMMA (CM-205)	DMSO	H_2O	Instantaneous liquid–liquid phase demixing	[35]
DMSO	PVDF (Kynar 740)/PMMA (CM-205)	DMSO	H_2O	Delayed liquid–liquid phase demixing	[35]
DMSO	CA (E 398–3)	DMSO	H_2O	Delayed liquid–liquid phase demixing	[36]
DMAc	CA (E 398–3)	DMAc	H_2O	Delayed liquid–liquid phase demixing	[36]
Acetone	CA (E 398–3)	Acetone	H_2O	Delayed liquid–liquid phase demixing	[36]
Dioxane	CA (E 398–3)	Dioxane	H_2O	Delayed liquid–liquid phase demixing	[36]
CO_2-III	PVDF (Solef 1015)	DMAc	H_2O	Instantaneous liquid–liquid phase demixing	This
CO_2-III	PVDF (Solef 1015)	NMP	H_2O	Delayed liquid–liquid phase demixing	study
CO_2-III	PVDF (Solef 1015)	DMF	H_2O	Delayed liquid–liquid phase demixing	

[a] AA-$NaHCO_3$, acetic acid-sodium bicarbonate; DMSO, Dimethyl sulfoxide; DCM, Dichloromethane; PVDF, Poly (vinylidene fluoride); PVDF-HFP, Poly(vinylidene fluoride-co-hexafluoropropylene); CA, Cellulose acetate; PES, poly(ether sulfone); TEP, N,N-Triethyl- phosphate; EVAL, Poly(ethylene-co-vinyl alcohol); PSf, Polysulfone; IBA, butyl acetate; EA, ethyl acetate; BA, Butyl acetate; S-PPSU, Sulfonated Polyphenylsulfone; PBI, Polybenzimidazole; Rhodiasolv Polarclean, Methyl-5-(dimethylamino)-2-methyl-5-oxopentanoate; Na_2SO_4, Sodium sulfate; KOH, Potassium hydroxide; CA, Cellulose acetate; PU, Polyurethane; PVA, Poly(vinyl alcohol); PAN, Polyacrylonitrile; PI, Polyimide; PC, Polycarbonate; NMMO, N-methylmorpholine-N-oxide; i-BuOH, Isobutanol; MeOH, Methanol; EtOH, Ethanol; i-PrOH, Isopropanol; PrOH, n-propanol; BuOH, n-butanol; IPOH, Isopropanol; IBA, Isobutyl alcohol; IPA, Isopropyl alcohol; BA, Butyl acetate; EA, Ethyl acetate; t-BuOH, t-Butanol; NaOH, Sodium hydroxide; 6FDA, 4,4′ hexafluoroisopropylidene diphtalic anhydride; 4,4′ODA, 4,4′-oxydianline.

1. Introduction

Membranes are commonly fabricated as flat sheets or as hollow fibers with asymmetric, symmetric, multilayered, or bi-layered cross-sectional structures [1]. They are generally made from organic polymers, inorganic polymers, or composite materials [1]. Various methods exist for fabricating membranes including interfacial reactions, sol–gel processes, extrusion, etching, stretching, and polymer phase separation [2]. The nonsolvent phase inversion technique (NIPS) is one of the most widely used fabrication methods due to its simplicity and scalability [1,3]. Membrane formation via NIPS proceeds via the exchange of a solvent in a polymeric solution with a non-solvent or coagulant [4]. The demixing of the polymer solution during the NIPS process governs the ultimate structural form of the membrane, which depends strongly on the kinetics and thermodynamics of the phase inversion process.

The coagulation medium plays a key role in membrane formation during NIPS processes. Therefore, the nonsolvent's effect on the membrane's final morphology has been investigated by using different coagulation media and nonsolvent additives. Table 1 lists some of the most notable types of coagulation media and nonsolvent additives for membrane fabrication using NIPS. Although water is the most commonly used nonsolvent, it has the drawback of being harsh towards widely used solvents in membrane fabrication such as NMP, DMAc, and DMF. Using a nonsolvent additive is therefore an attractive strategy for tuning the affinity between solvent and nonsolvent and tailoring the morphology of the final polymeric membrane. Alcohols are the most widely studied class of nonsolvent additives in membrane formation by NIPS. The nonsolvent properties of water can also be manipulated by using CO_2 as a nonsolvent additive. This strategy is attractive because it is sustainable and readily scaled up using carbonation equipment, and also provides a way of productively utilizing captured carbon dioxide.

The need of treating radioactive wastewater has received increased attention since the Fukushima accident in 2011, which emphasized the requirement of reliable methods of removing radioisotopes from wastewater to support the sustainable development of the nuclear power industry while protecting the environment and human health. Radioactive liquid waste originates from several sources, including nuclear power plants, industrial facilities producing radioisotopes, uranium enrichment plants, nuclear weapons research sites, radiopharmaceutical research centers, laundry wastewater from nuclear sites, and radioisotopes used in medical procedures. Consequently, the handling of radioactive liquid waste is a major concern.

Nuclear wastewater requires treatment to comply with discharge regulations and minimize the stored volume of radioactive material. Various treatment methods have been developed and applied for this purpose, including thermal evaporation, chemical precipitation, ion exchange, and methods using membranes either alone or in combination with other physicochemical techniques to remove radionuclides from

real and simulated radioactive wastewaters. Notable membrane-based methods include reverse osmosis (RO), RO with ultrafiltration (UF) pretreatment, and a combination of complexation with UF/nanofiltration (NF). [37-40]. Conventional treatment methods are limited by their inability to fully eliminate contaminants, high operating costs, and the large quantities of secondary solid waste produced, which hinders satisfactory treatment of nuclear waste.

As an alternative, MD separation process can achieve high rejection with low energy consumption and reduced equipment costs when treating radioactive wastewater. Moreover, MD is a thermal process, which may be beneficial since nuclear power plants generate large amounts of waste heat that could be exploited to drive MD processes. Khayet [41] proposed a DMCD technique based on membranes modified with surface-modifying macromolecules (SMM) to treat wastewater with radioactive isotopes containing ^{60}Co, ^{137}Cs and ^{85}Sr, which had a very high rejection rate, and the radioactive activity of the generated distillate was even at the natural background level. Jia et al. [42] developed an automatically operated pilot-scale VMD demonstration plant for the purification of cesium ions in simulated radioactive wastewater. The results showed that the DF of Cs^+ reached $10^{4.85}$. Nie et al. [43] used a polytetrafluoroethylene (PTFE) hollow fiber membrane combined with VMD technology to treat low-level radioactive wastewater containing uranium, showing excellent retention capacity for all major pollutants in the wastewater, meeting China's discharge standard. Dytnerskii et al. [44] performed a series of experiments using direct contact membrane distillation (DCMD) to process radioactive wastewater and promising results were obtained with a DF range of 90–11,000 for ^{137}Cs. Zakrzewska-Trznadel et al. [45] performed similar experiments and the results showed that most of the radionuclides such as ^{65}Zn, ^{110}Ag, ^{133}Ba, ^{134}Cs, ^{170}Tm and ^{192}Ir from the radioactive feed were not detected in the permeate with theoretically infinite DF, while the DF of ^{60}Co and ^{137}Cs were 43.8 and 4336.5, respectively. Most of the radionuclides in the feedstock liquid can reach an undetected level in the distillate, demonstrating that MD can be used to treat radioactive wastewater of different levels.

In this work, CO_2 is presented as a novel nonsolvent additive for membrane fabrication from PVDF using the most popular solvents in the membrane industry: NMP, DMAc, and DMF. The impact of the CO_2 concentration in coagulation bath on the phase inversion process and the morphology, physical properties, and permeability of the fabricated membranes was investigated. The best performing membranes were then tested in DCMD and AGMD configurations for nuclear wastewater decontamination.

2. Experimental

2.1. Chemicals

PVDF (Solef 1015, $M_W = 534000\ g{\cdot}mol^{-1}$) was kindly supplied by Solvay Specialty Polymers. NMP, DMAc, DMF, kerosene (used as a wetting agent for ε measurement), NaCl (99%), $NaNO_3$ (>99%), CsCl (>98%), $CrCl_3{\cdot}6H_2O$ (96%), and $Co(NO_3)_2{\cdot}6H_2O$ (>98%) were purchased from Sigma–Aldrich Chemical Co. All chemicals were used without further purification. Stock solutions of cesium (Cs), cobalt (Co), and chromium (Cr) (1000 mg/L in 2.5% HNO_3) were obtained from CPI international (Amsterdam, Netherlands) and used to prepare the standard solutions for preparation of calibration curves.

2.2. Carbonating the coagulation bath

Carbonated coagulation baths were prepared with three CO_2 concentrations (low, medium, and high) at a temperature of 20 °C using distilled water and a PWR-001 machine supplied by SodaStream USA, Inc. The amount of dissolved CO_2 in water samples was determined by titration of precipitated barium carbonate with hydrochloric acid and sodium hydroxide solutions as detailed in SI [46,47].

2.3. CO_2 solubility and concentration determination

The solubility of CO_2 in DMF, DMAc, and NMP was measured at 298.15 K and pressures of up to 2 MPa using a vapor–liquid equilibrium (VLE) setup according to the protocol described in the supporting information (see S1.1). Again, titration of precipitated barium carbonate using hydrochloric acid and sodium hydroxide solutions was used to quantify the amount of CO_2 dissolved in the coagulation bath, as detailed in the supporting information (see S1.2).

2.4. Polymer solution

To eliminate possible residual moisture, PVDF powder was dried overnight under vacuum at 80 °C before use. The dried powder was then mixed with the desired solvent (NMP, DMAc, or DMF) to the desired concentration (10, 12.5, or 15 wt%) and the mixture was stirred at 60 °C until homogeneous. Three polymer batches were prepared for each composition to ensure the reproducibility of the obtained experimental data.

2.5. Membrane preparation protocol

Polymer solutions were cast at room temperature with a defined thickness of 150 μm using an automated film applicator (Elcometer 4340). The nascent membranes were precipitated immediately by immersing the polymer film into a coagulation bath at 20 °C containing a predetermined concentration of CO_2 as a coagulation additive. The samples were immersed in the coagulation bath long enough to ensure complete exchange of solvent and non-solvent, leading to self-initiated detachment of the membrane from the glass support. The samples were then transferred to another bath containing distilled water and stored for 24 h to extract the residual solvent from the membrane structure. Finally, the membranes were stored in air-tight bags containing 20% glycerol in distilled water to prevent pore collapse.

2.6. Cloud point measurements

Cloud point determination was performed for all solvent systems using coagulation baths containing distilled water and three concentrations of CO_2. A common titration method was used to determine the cloud point in the ternary phase diagram of the PVDF/solvent/nonsolvent systems [48]. Under constant stirring, water was added dropwise (50–100 μL) to each dope solution, resulting in a local phase inversion at the contact point of the water and the dope system. The polymer system was stirred continuously, causing water to diffuse through the entire solution, leading to the restoration of homogeneity and the disappearance of the local turbidity that formed when the water droplet first struck the dope solution. Another drop of water was then added with continuous stirring, and the process was continued until the solution became persistently cloudy and/or exhibited evidence of gelation, indicating phase separation had occurred. The composition of the system at that point was then plotted on a ternary phase diagram to obtain the experimental binodal line. This line was determined for all PVDF/solvent/water (distilled or carbonated) systems.

For ternary nonsolvent/solvent/polymer systems, the cloud point composition of the PVDF polymer solution could also be interpreted based on the correlation (Eq. S2) of the linearized cloud point curve (LCP) according to Boom *et al.* [48].

2.7. Mutual diffusion coefficient and solubility parameter calculations

The diffusion coefficient D_{AB} in Fick's law represents the diffusion rate of a component in the medium and measures the medium's transport capacity. The diffusion coefficient of solvents can be calculated using the Wilke-Chang equation [49]:

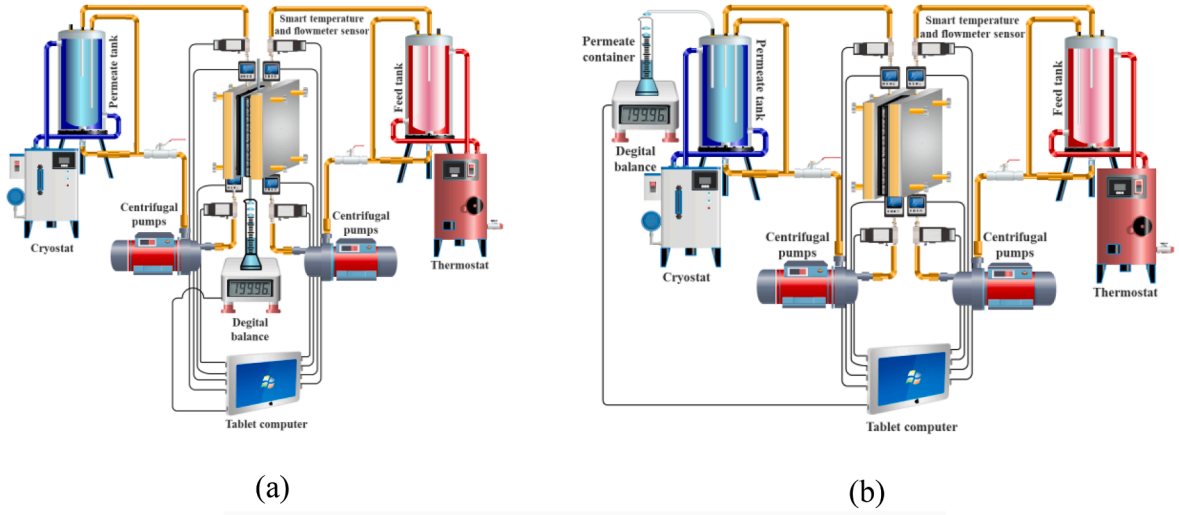

Fig. 1. a) Air Gap Membrane Distillation (AGMD) setup, b) Direct Contact Membrane Distillation (DCMD) setup.

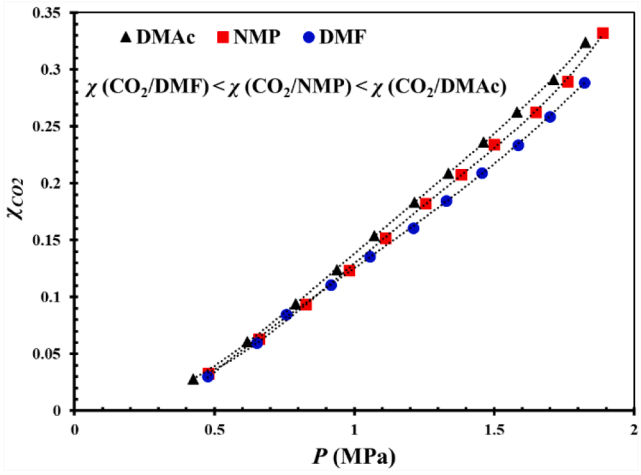

Fig. 2. The solubility of CO_2 at $T = 25$ °C in DMAc, NMP and DMF.

$$D_{AB} = 7.4 \times 10^{-15} \frac{(\varphi M_B)^{1/2} \times T}{\mu \times V_A^{0.6}} \quad (1)$$

Here, $D_{AB}(\frac{cm^2}{s})$, is the diffusion coefficient of solute A in solvent B; T (K) is the temperature of the solution; $\mu(Pa.s)$ is the viscosity of solvent B; M_B (kg/kmol) is the molecular weight of the solvent B; φ is the association factor, which takes values of 2.3 and 1.1 for $D_{S\text{-}W}$ and $D_{W\text{-}S}$, respectively; and V_A (cm^3/mol) is the molecular volume.

The polymer–solvent affinity can be estimated by introducing the "solubility parameter", δ, defined as the square root of the cohesion energy density, which describes the strength of attraction between the molecules. For casting solutions, polymer–solvent interactions were evaluated based on the difference in the solubility parameters between the polymer and the solvents. The solubility parameters (δ) of solvents and polymers can be defined as [50,51]:

$$\delta = \sqrt{\delta_d^2 + \delta_p^2 + \delta_h^2} \quad (2)$$

where, δ_d, δ_p and δ_h represent the contributions of dispersive interactions (d), polar bonds (p) and hydrogen bonds (h), respectively. The solubility parameters of PVDF (P) and the solvents (S) together with the values of the mutual diffusion coefficients are shown in Table S3.

2.8. Membrane characterization

The morphology of the fabricated membranes was analyzed with a field emission scanning electron microscope (FESEM, JOEL Model JSM-6330F). Samples for cross-section analysis were prepared by fracturing in liquid nitrogen, mounted on the sample holder using double-sided carbon adhesive tape, and sputtered with gold using a rotary-pumped sputter coater (QUORUM Q150R S) for 60 s at 20 mA.

Bulk ε was evaluated by measuring the weight of samples before and after infiltration with the pore-penetrating agent kerosene. Three measurements were performed using samples with a surface area of approximately (4 × 1.5) cm^2 for each membrane. After measuring the weight of the dry membrane (W_D), the samples were immersed in kerosene for 24 h, after which the samples were removed, their surfaces were gently wiped with tissue paper to remove superficial kerosene droplets, and they were weighed (W_W). The ε was then evaluated based on the weight of the dry membrane, W_D, and the wet membrane, W_W, the density of kerosene at room temperature ($\rho_k = 0.81$ g/cm^3), and the density of PVDF (1.78 g/cm^3). The formula used for ε determination is given in equation (3), where ρ_p represents the density of pure PVDF.

$$\varepsilon(\%) = \frac{\frac{W_w - W_d}{\rho_k}}{\frac{W_w - W_d}{\rho_k} + \frac{W_d}{\rho_p}} \times 100 \quad (3)$$

The pore size distribution and the mean pore size were determined using a gas–liquid displacement capillary flow porometer (CFP; POROLUX 100, IB-FT Germany) with POROFIL125 as the liquid wetting agent as described previously [52]. The liquid entry pressure of water (LEP_w) for the membranes was determined using distilled water following a published procedure [52,53]. Measured mean values and standard deviations are presented for three different membrane samples.

Tensile strengths (MPa) and elongation ratios (%) were measured with a tensile testing machine (MODEL SH-20, Wenzhou Shandu Instrument Co., China) at a loading rate of 50 mm·min^{-1}. The reported values are means for five test runs.

Fourier transform infrared (FTIR) spectra of the fabricated PVDF membranes were acquired using a Bruker spectrometer (Vertex 80) over the range of 600–1600 cm^{-1} at a resolution of 2 cm^{-1} in ATR (attenuated total reflection) transmission mode.

2.9. Pure water permeability (PWP) and membrane distillation (MD)

Before examining the fabricated membranes' performance in decontamination and desalination by MD, microfiltration experiments

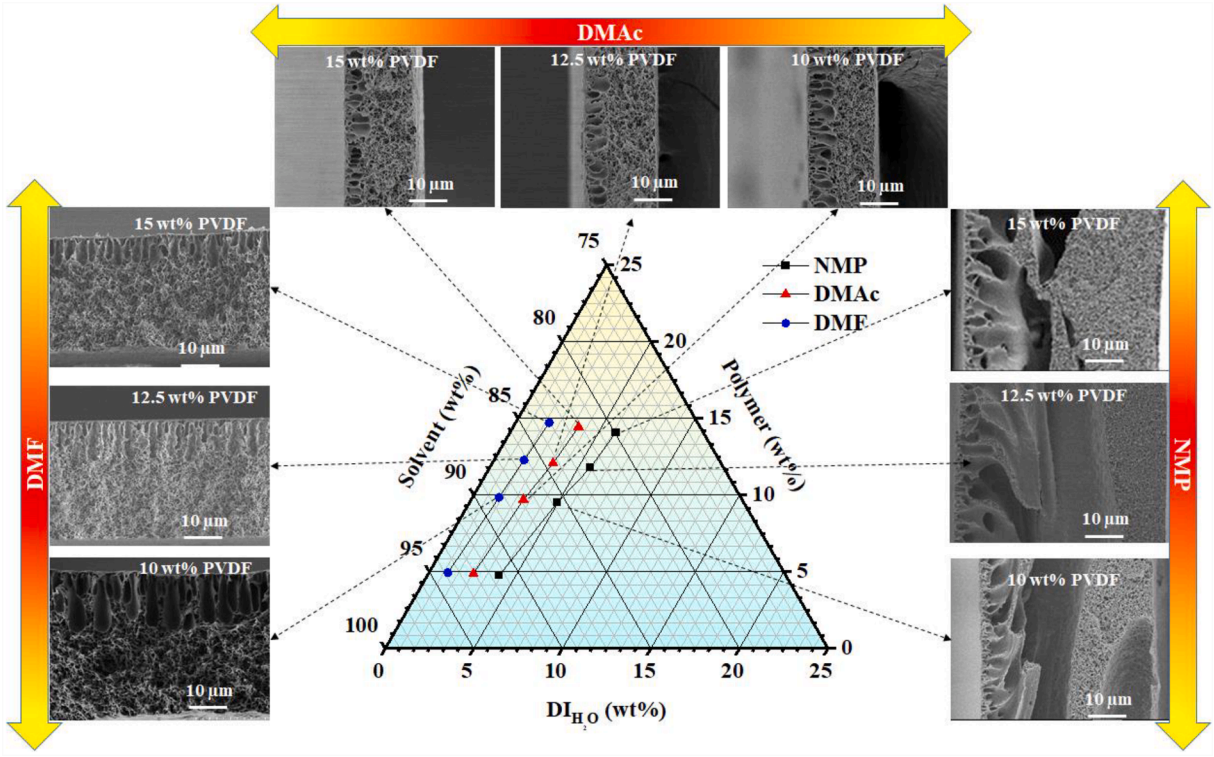

Fig. 3. The cloud point lines of PVDF/solvent/water systems at room temperature and SEM images membranes obtained at different cloud points.

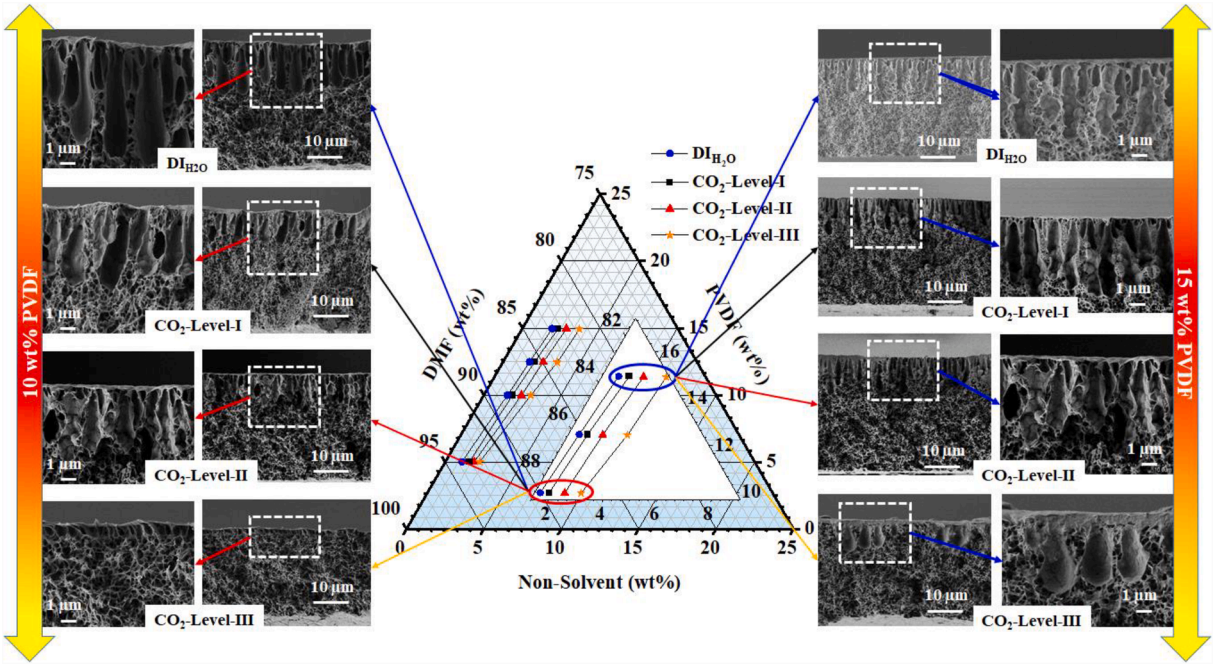

Fig. 4. The cloud point lines of PVDF/DMF/water systems at room temperature and SEM images of the resulting membranes.

were performed with distilled water to measure the membranes' *PWP*. This was done using a dead-end filtration setup. Distilled water at 25 °C was pumped through the membrane, for which the effective diameter of the filtration area was 40 mm. Initial stabilization was carried out for 30 min. at a transmembrane pressure of 1 bar, after which the permeate water was collected. Three replicate measurements were performed for each combination of membrane fabrication conditions. The *PWP* ($kg{\cdot}m^{-2}{\cdot}h^{-1}{\cdot}bar^{-1}$) was determined using the following equation:

$$PWP = W/S.\Delta t.P \quad (4)$$

Here, W (kg) is the weight of the permeate water, S (m^2) is the effective membrane area, Δt (h) is the collection time, and P (bar) is the applied pressure.

Fig. 1 presents schematic depictions of the experimental apparatus for DCMD and AGMD. The setup consists mainly of a PVDF flat sheet membrane module (model CPR920, Convergence Industry B.V;

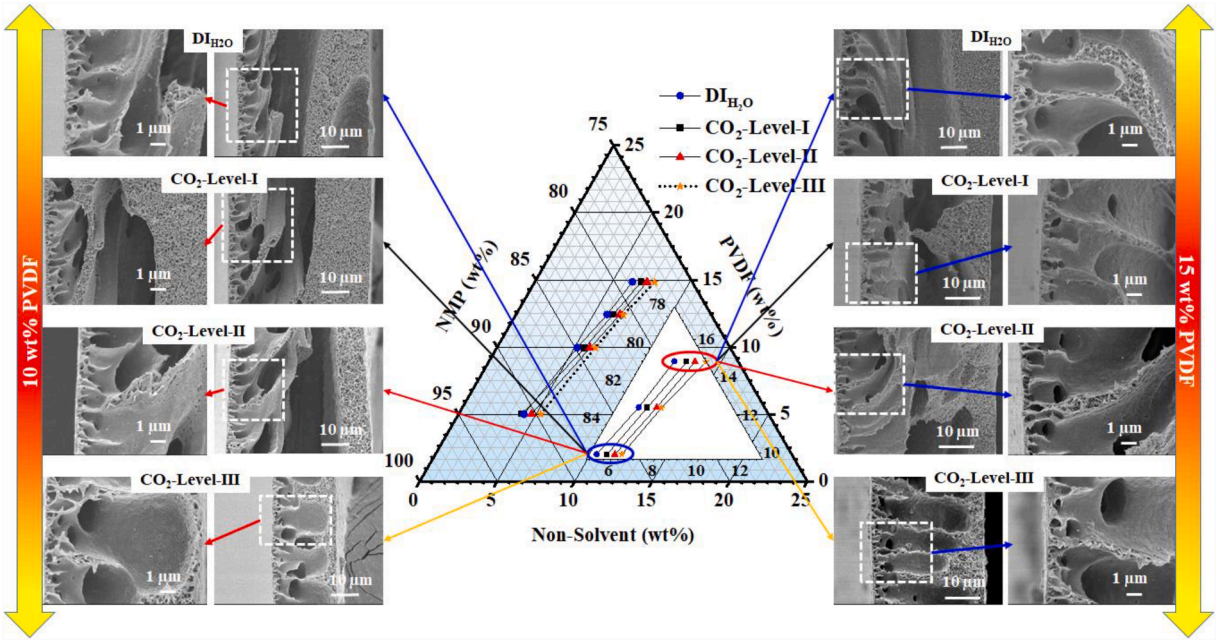

Fig. 5. The cloud point lines of PVDF/NMP/water systems at room temperature and SEM images of the resulting membranes.

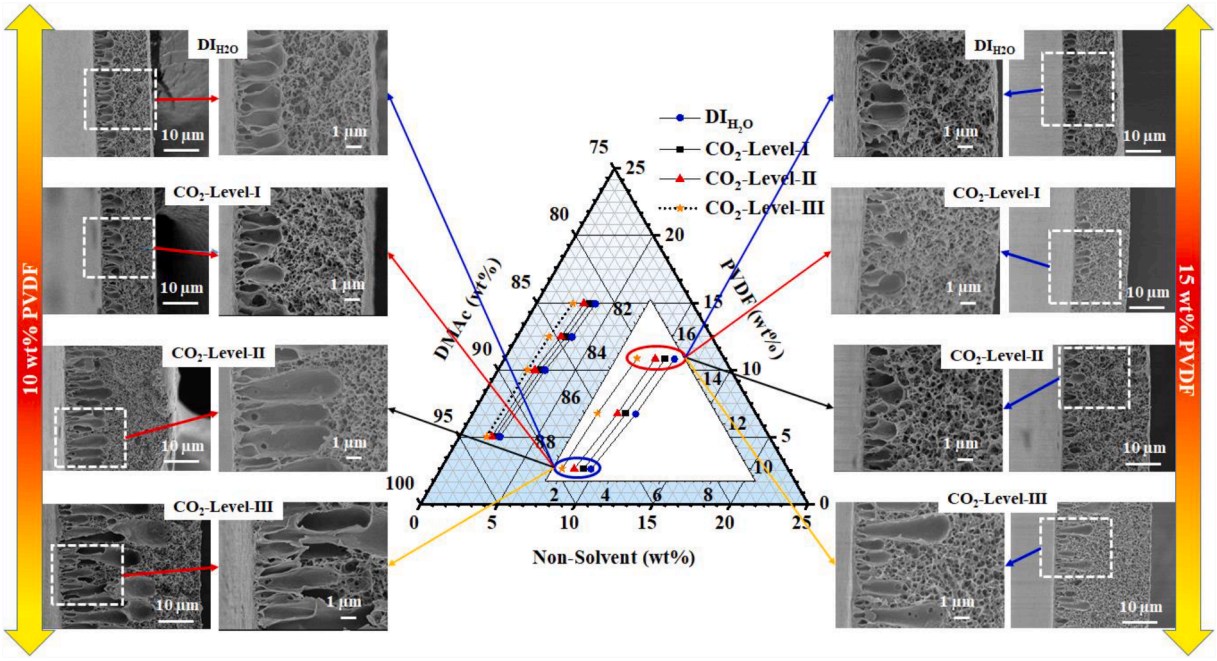

Fig. 6. The cloud point lines of PVDF/DMAc/water systems at room temperature and SEM images of the resulting membranes.

Netherlands) with an effective surface area of 0.006 m^2 (0.04 m wide and 0.15 m long), feed and distillate containers ($V = 1$ dm^3) and two magnetic Coupling Water Pumps (Xylem Flojet, HPR6/8, Totton Pumps Ltd, UK). Two flow meters and four TMU thermometers (Papouch store s.r.o.; Czech Republic) were installed at the inlets and outlets of the membrane module and were connected to a computer via USB interfaces, allowing automated recording of the inlet and outlet temperatures every 30 s. Both air gap membrane distillation (AGMD, Fig. 1a) and direct contact membrane distillation (DCMD, Fig. 1b) were performed using this apparatus. In the system, two solutions with different temperatures are concurrently circulated in direct contact with the hydrophobic membrane through separate channels. The feed solution (SNWW or a solution of NaCl or $NaNO_3$) flowed through the active layer of the membrane, and the distilled water was recirculated on the porous support side of the membrane in the case of DCMD or the metal plate in the case of AGMD. In both cases, the circulation of the fluids was driven by magnetic pumps.

2.10. Experimental procedures

CsCl, $CrCl_3{\cdot}6H_2O$, $Co(NO_3)_2{\cdot}6H_2O$, and $NaNO_3$ were used to prepare simulated radioactive nuclear wastewater (SNWW) [42,54]. The simulated solution contained approximately 450 ppm of each of Cs^+, Cr^{3+}, and Co^{2+}, to which 35 g/L $NaNO_3$ was added. $NaNO_3$ was chosen because it is commonly present in natural radioactive wastewater.

At the start of each experiment, DCMD was performed for 3 h using

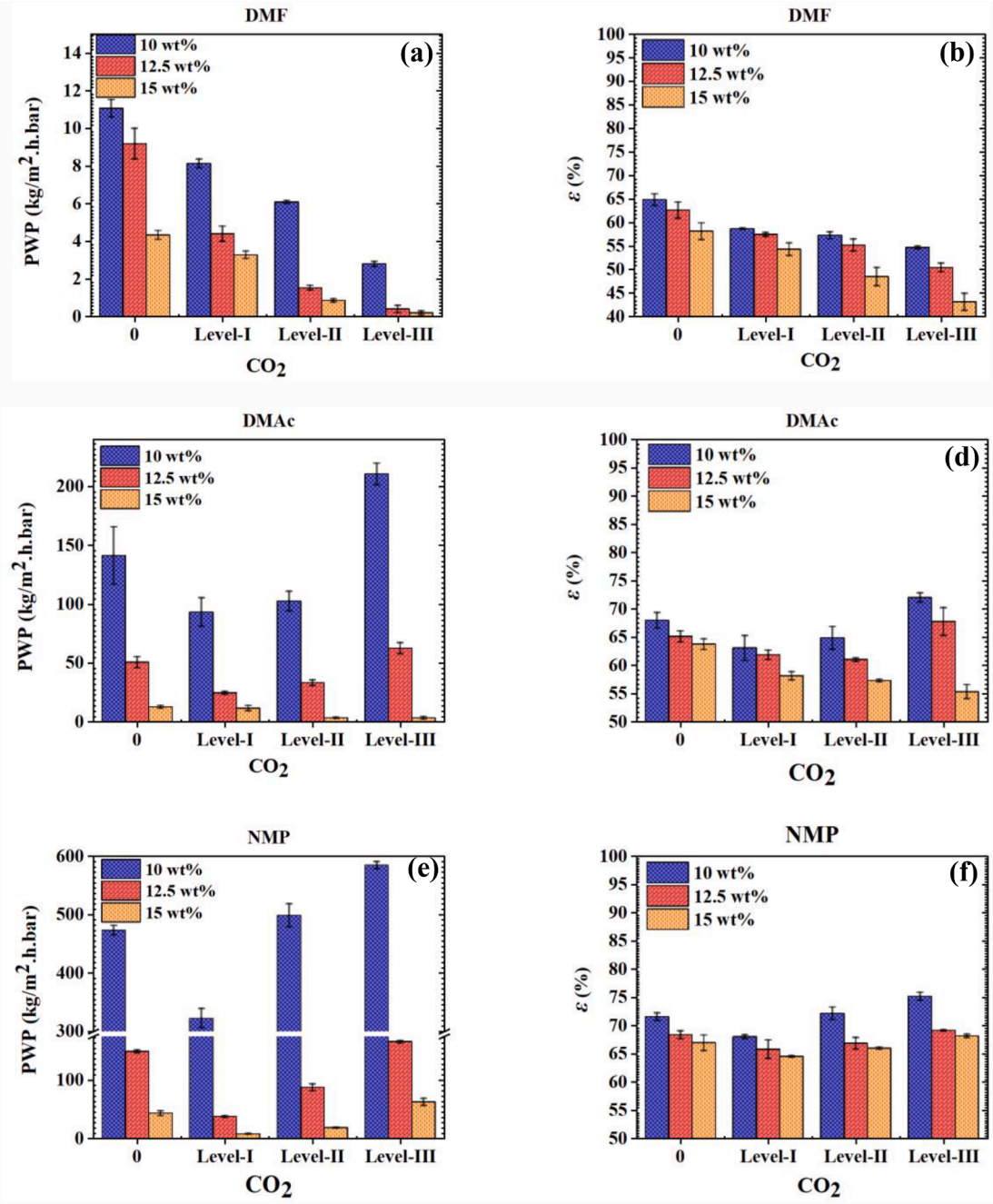

Fig. 7. PWP and ε values for PVDF membranes fabricated from polymer solutions of different concentrations in DMF, DMAc, and NMP using coagulation baths with different CO_2 concentrations.

distilled water as both feed and permeate to check for leakage or defects in the membrane or module. DCMD was then performed for another 3 h using a 35 g/L NaCl aqueous solution as the feed and distilled water as the permeate, and for another 3 h using a 35 g/L aqueous solution of $NaNO_3$ as the feed with distilled water as the permeate. DCMD (6 h) and AGMD (4 h) experiments were then performed using SNWW with the composition specified above. To identify possible fouling and/or changes in membrane performance during the experiments, the J_p was measured after each desalination experiment, using distilled water as feed and permeate under the same operating conditions as in DCMD for 3 h. The total operating times of the MD experiments with each PVDF flat sheet membrane were at least 28 h. The $T_{p,in}$ and $T_{f,in}$ were set to 20 °C and 70 °C, respectively, and were maintained within ± 0.5 °C of these values. The feed and permeate flow rates were kept constant at ~0.75 and 0.55 $L{\cdot}min^{-1}$, respectively.

The concentrations of Cs^{+}, Cr^{3+}, and Co^{2+} ions in the feed and permeate solution were determined using an inductively coupled plasma optical emission spectrometer (ICP-OES, PerkinElmer, Uberlingen, Germany), equipped with a cross-flow nebulizer. Elemental analysis was performed using a double spray chamber. Electrical conductivity was measured using an electrical conductivity monitor (edge, model HI2003, Hanna instruments Inc., USA) to determine the salt (NaCl and $NaNO_3$) content of the feed and permeate solutions.

The DCMD and AGMD treatment efficiencies for the aqueous salt and (SNWW) solutions were determined by calculating α and *DF*. The α [55] is defined by the following equation:

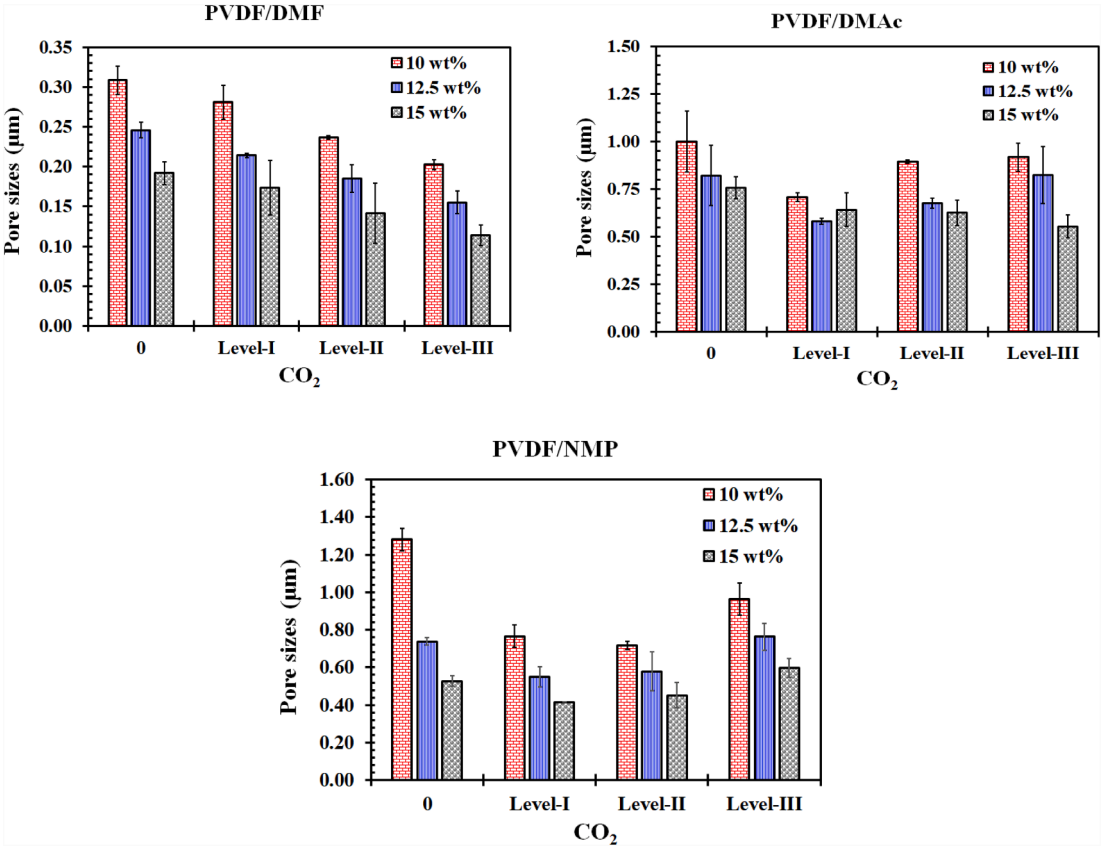

Fig. 8. Mean pore size of the prepared PVDF membranes as a function of polymer concentration and the CO_2 concentration of the coagulation bath.

$$\alpha(\%) = \left(1 - \frac{C_p}{C_f}\right) \times 100 \tag{5}$$

where C_f (g/L) and C_p (g/L) represent the salt concentrations of the feed and the permeate, respectively.

To avoid bias arising from the effect of dilution in the permeate tank when calculating the α, the permeate concentration was corrected using the following equation [56,57]:

$$C_p = \frac{C_1 m_1 - C_0 m_0}{m_1 - m_0} \tag{6}$$

where m_0 and m_1 represent the initial and final weight of the solution in the permeate tank, respectively, and C_0 and C_1 represent the initial and final salt concentration of the salt solution in the permeate tank, respectively.

The *DF* is calculated using the following expression:

$$DF = \frac{C_{f,i}}{C_{p,i}} \tag{7}$$

$$DF(\%) = (1 - \frac{C_{p,i}}{C_{f,i}}) \times 100 \tag{8}$$

where $C_{f,i}$ (ppm) is the measured concentration of nuclides in the feed solution and $C_{p,i}$ (ppm) is the concentration of nuclides in the permeate water. The index i refers to the ion under consideration (in this work, Cr^{3+}, Co^{2+}, or Cs^{+}).

3. Results and discussion

3.1. Solubility and concentration of CO_2

As shown in Table S1 and Fig. 2, the experimentally determined the mole fraction of CO_2 in DMF, NMP, and DMAc increased in the following order: χ (CO_2/DMF) < χ (CO_2/NMP) < χ (CO_2/DMAc). As a result, the amount of carbonated water needed to induce phase separation of dissolved PVDF would be expected to decrease in the order DMF > NMP > DMAc. The concentration of CO_2 in the coagulation baths (low, medium, and high) during PVDF membrane fabrication is shown in Table S2.

3.2. Phase diagrams and morphology

Analysis of the ternary phase diagram is an essential first step when studying polymer/solvent/nonsolvent interactions. In addition, thermodynamic analysis is important for understanding why specific morphologies emerge during membrane formation. A typical three-component phase diagram for NIPS membrane fabrication has two notable regions within its triangular area [2] – one representing a homogeneous single-phase polymer solution and another, separated from the first by the binodal curve, representing a biphasic region in which the ternary mixture spontaneously separates into polymer-rich and polymer-lean phases.

Experimental cloud point measurements for the PVDF/NMP/water, PVDF/DMAc/water, and PVDF/DMF/water systems at room temperature with polymer concentrations ranging from 5 wt% to 15 wt% are shown in Fig. 3. For these systems, the PVDF/DMF/water cloud point curve was closest to the polymer–solvent axis and thus had the largest demixing gap, while the PVDF/NMP/water cloud point curve was closest to the polymer-coagulant axis and thus had the smallest demixing gap. In other words, only a small amount of water is needed to disturb the equilibrium of the PVDF/DMF/water system and induce polymer precipitation, and phase inversion occurs earlier than in the system with NMP. Moreover, as shown in Figure S1, the correlation coefficients of the LCP curves at 25 °C are above 0.99 for the studied solvent systems, indicating that only liquid–liquid demixing occurs. The

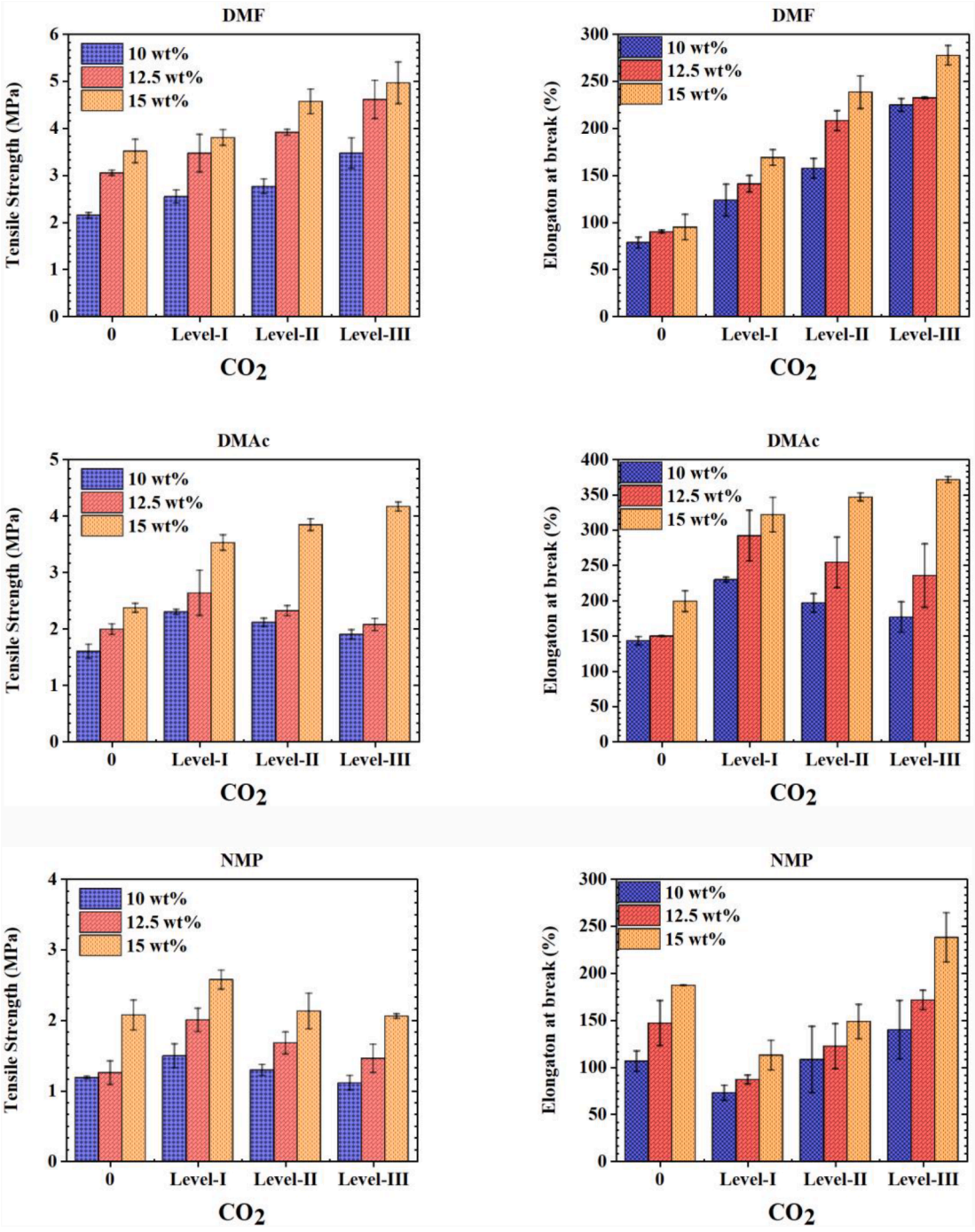

Fig. 9. Stress–strain data for PVDF membranes as functions of the polymer concentration in the casting solution and the CO_2 concentration in the coagulation bath.

value of the *b* term increased (slightly) in the following order: *b*(DMF) < *b*(DMAc) < *b*(NMP), indicating that the coagulation potential of the (PVDF/NMP) system was lower than that of the (PVDF/DMF) system. Consequently, the thermodynamic stability of the solvent/PVDF systems (and thus the amount of nonsolvent required to induce precipitation) increased in the order DMF < DMAc < NMP. The phase boundaries determined in this work are consistent with previous reports [58].

In accordance with the different thermodynamic stabilities of the solvent systems, the amount of water needed to induce phase separation differed significantly between them; phase separation occurred at a water content of 4–7 wt% in the NMP system and 1–2 wt% in the DMF system. As a result, the structures of the obtained membranes depended on the choice of solvent.

Several parameters affect the final membrane structure in the phase inversion process. Among the most critical important are the choice of solvent and nonsolvent, the concentration of the casting solution, the temperature of the coagulation bath, and the location of the demixing gap [2]. Various membrane formation pathways exist in the ternary phase diagram, resulting in different morphologies. Upon immersing the casting solution in a coagulation bath, demixing will occur by one of two mechanisms: instantaneous demixing or delayed demixing.

The morphology of polymeric membranes fabricated by phase inversion depends on both thermodynamic and kinetic factors. According to the principles of equilibrium thermodynamics, the greater the difference between the solubility parameters of the polymer and the solvent ($\delta_{p\text{-}s}$), the lower the solvent's ability to dissolve the polymer and

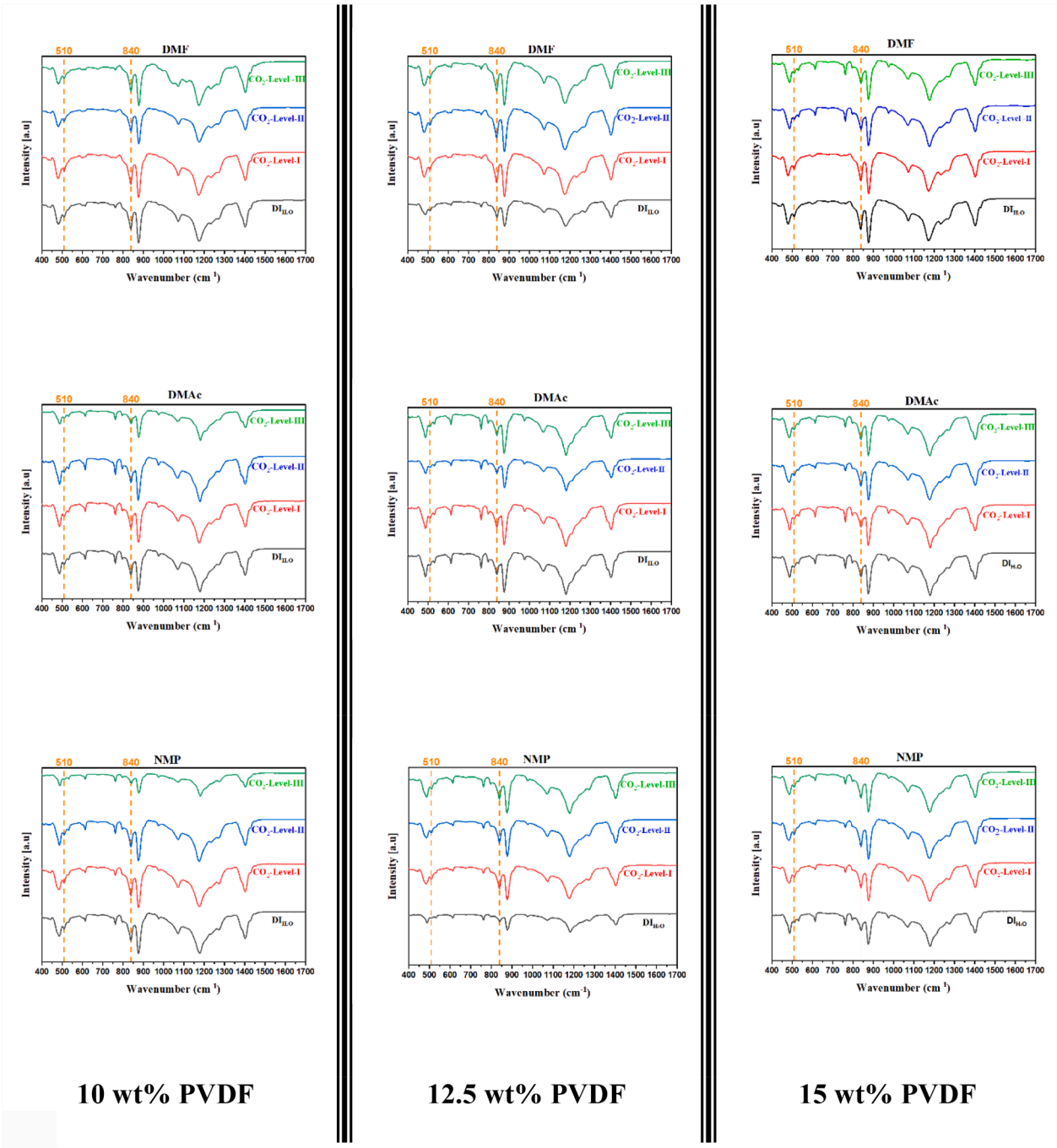

Fig. 10. FTIR ATR spectra of PVDF membranes fabricated with different solvents, polymer concentrations, and CO_2 concentrations in the coagulation bath.

the lower the stability of the polymeric casting solution, leading increased formation of finger-like cavities in the final membrane [51]. However, the observed structures of the fabricated membranes (see Fig. 3) were inconsistent with these expectations. This can be attributed to the influence of kinetic factors.

The mutual diffusivities of the solvent/nonsolvent systems are shown in Table S3. Importantly, the difference between the rates of nonsolvent inflow and solvent outflow is much smaller for the NMP/water system than for the DMF/water and DMAc/water systems, i.e. $(D_{water-DMF} - D_{DMF-water}) \approx (D_{water-DMAc} - D_{DMAc-water}) \gg (D_{water-NMP} - D_{NMP-water})$. Therefore, in the DMF and DMAc systems, water readily penetrates into the membrane structure and limits macrovoid growth. Conversely, the rates of water inflow and solvent outflow are similar in the NMP systems, leading to greater macrovoid formation.

Membranes prepared in NMP generally had asymmetric structures with irregularly shaped macrovoids under the skin layer. Those prepared in DMAc or DMF were also asymmetric but had a thin skin layer with short underlying finger-like voids supported by a sponge-like structure.

To investigate the effect of the polymer concentration in the casting solution, membranes were prepared using different concentrations of PVDF (10, 12.5, and 15 wt%) in distilled water baths at 20 °C. At 10 wt% PVDF/NMP, instantaneous demixing occurs due to severe nonsolvent (i.e. water) inflows and solvent outflows throughout the membrane, resulting in the formation of large finger-like macrovoids. That is to say, the kinetic factors of phase inversion are more important than thermodynamic factors in this case. In contrast, macrovoid formation is

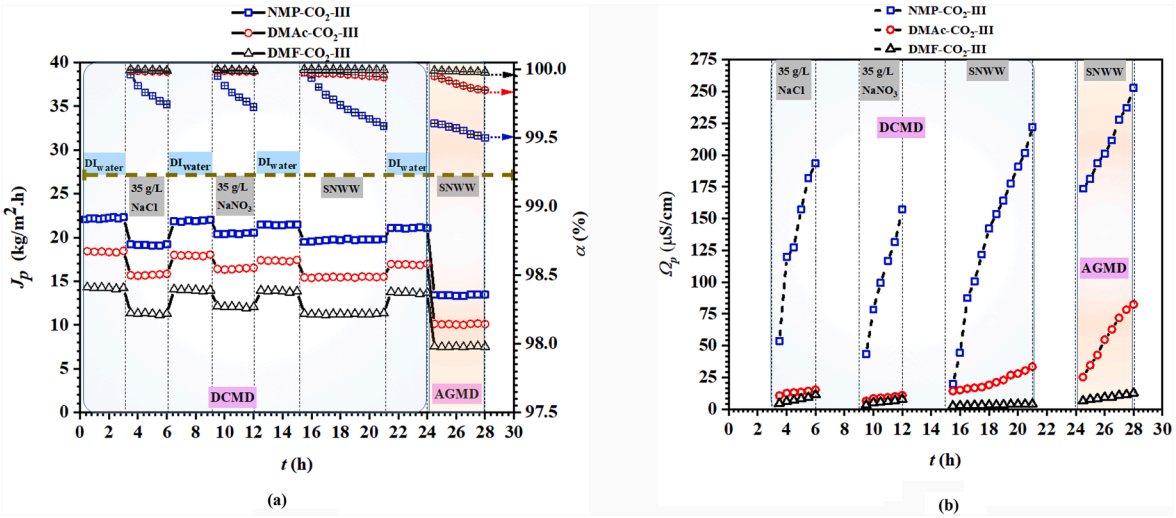

Fig. 11. a) Results from MD experiments with aqueous salt solutions and simulated nuclear wastewater (SNWW), b) variation of the permeate's electrical conductivity during MD tests.

suppressed in the PVDF/DMAc and PVDF/DMF membranes, which have sponge-like cross-sections when fabricated at the same polymer concentration. Kinetic factors favor the formation of sponge-like pores if the solvent's diffusion coefficient in water is low, which was confirmed to be the case for DMAc and DMF (see Table S3).

Raising the polymer concentration from 10 to 15 wt% (Fig. 3) suppressed water intrusion to some extent, reducing the size of the finger-like macrovoids in the top layer of the membrane. This can be attributed to the higher viscoelasticity of more concentrated polymer solutions, which prevents immediate convective-type solvent exchange during instantaneous liquid–liquid phase separation processes [4]. Increasing the polymer concentration in the casting solution also reduced the number of macrovoids and changes their shape, making them teardrop-like rather than finger-like in the PVDF/DMAc and PVDF/DMF systems. In the PVDF/NMP system, large fingers supported by a spongy macroporous wall were formed. These outcomes can be explained by considering kinetic factors: the increase in viscosity caused by raising the concentration of the polymer in the casting solution slows down demixing but not enough to prevent the formation of finger-like structures. Furthermore, the longer finger-shaped voids seen in the cross-sections of the membrane prepared with the PVDF/NMP system (Fig. 3) suggests that lower PVDF concentrations favor instantaneous liquid–liquid demixing, which may result in a trend towards a larger average pore size at the surface and high porosity.

The coagulation media also plays a key role in controlling liquid–liquid demixing and crystallization during PVDF membrane formation by immersion precipitation. Water is a strong nonsolvent of PVDF, so the use of water as the coagulation medium during immersion precipitation often causes rapid liquid–liquid demixing that produces membranes with asymmetric structures featuring finger-like voids as seen in Fig. 3 [4].

Fig. 4 shows cross-sectional images of membranes prepared using the PVDF/DMF system together with the corresponding cloud point measurements obtained using distilled water and carbonated water with three CO_2 concentration levels (low, medium, and high), corresponding to CO_2 concentrations (levels I, II, and III, respectively).

PVDF membranes prepared with distilled water as the nonsolvent exhibit a typical asymmetric structure with a thin, dense skin layer over a porous layer containing independent finger-like cavities enclosed in a solid porous matrix. When the PVDF concentration was 10 wt%, the finger-like cavities accounted for 39.7% of the visible area in the membrane precipitated with pure water but were completely absent in the membrane precipitated using carbonated water with the highest CO_2 concentration. Similarly, at a PVDF concentration of 15 wt%, the proportion of the membrane's thickness containing finger-like cavities fell from 35.9% when precipitation was performed with pure water to 27.5% at the highest CO_2 concentration in the coagulation medium.

Fig. 4 also shows that the demixing gap of the DMF/nonsolvent system increased in the order DMF/Level-III < DMF/Level-II < DMF/Level-I < DMF/water. That is to say, the demixing gap increased as the CO_2 concentration in the coagulation bath decreased. In addition, the cloud point curve shifted towards the polymer/nonsolvent axis as the CO_2 concentration in the coagulation bath increased, indicating that the coagulant became less effective at inducing phase inversion (or equivalently, the thermodynamic stability of the casting solution increased). This would be expected to reduce the rate of solvent/nonsolvent transport during membrane formation, so transport became slower as the CO_2 concentration in the coagulation bath increased. This is because the low solubility of CO_2 in DMF (see Fig. 1 and Table S1) reduced the affinity between the solvent (DMF) and nonsolvent coagulation bath. Consequently, a larger volume of nonsolvent was needed to induce phase separation, especially at higher CO_2 concentrations, and the thermodynamic stability of the PVDF/DMF/nonsolvent systems increased in the following order: water < CO_2-Level-I < CO_2-Level-II < CO_2-Level-III. Therefore, water is a strong nonsolvent for the PVDF/DMF system but becomes weaker as its level of carbonation increases.

The cross-sectional morphologies of asymmetric PVDF membranes prepared using NMP as the solvent with different CO_2 concentrations in the coagulation bath are shown in Fig. 5. When using distilled water without added CO_2 in the coagulation bath, a tilted finger-like structure was formed with large macrovoids supported on a sponge layer (bottom layer). In contrast, a narrower, vertical finger-like morphology supported on an underlying sponge layer was obtained when the PVDF/NMP system was precipitated using a carbonated coagulation bath. It was previously reported that using a single nonsolvent (water) as the coagulant resulted in the formation of finger-like morphologies in systems with high solvent/nonsolvent affinity and a suitable solvent for the polymer [51]. The formation of finger-like structure supported by a sponge-like layer with a large intermediate void in the PVDF/NMP/water system, and the narrow finger-like supported by a sponge-like layer in the PVDF/NMP/water system can be explained in terms of the interactions between the system's components and its phase separation kinetics.

Increasing the CO_2 concentration in the coagulation bath reduced the demixing gap of the PVDF/NMP/nonsolvent systems and shifted the cloud point curve towards the polymer/non-solvent axis. That is to say,

Table 2
Variation in the electrical conductivity of the permeate during DCMD/AGMD desalination of aqueous salt solutions and SNWW, LEP_w, pore diameter (d_p) and its distribution of the tested membrane.

Membrane	Configuration	Process	$\Omega_{p,i}$ (μS/cm)	$\Omega_{p,f}$ (μS/cm)	Time (h)	LEP_w (10^5Pa)	d_p (nm)
NMP-CO_2-III	**DCMD**	Desalination of 35 g/L NaCl	5.93	193.4	3	0.96	235.13
		Desalination of 35 g/L $NaNO_3$	±1.11	157.30	3	±0.11	±17.80
		Desalination of 450 ppm		222.10	6		
	AGMD	(Cs, Cr and Co) + 35 g/L $NaNO_3$	–	252.80	4		
DMAc-CO_2-III	**DCMD**	Desalination of 35 g/L NaCl	5.93	15.33	3	2.15	112.83
		Desalination of 35 g/L $NaNO_3$	±1.11	11.13	3	±0.27	±6.10
		Desalination of 450 ppm		33.53	6		
	AGMD	(Cs, Cr and Co) + 35 g/L $NaNO_3$	–	82.50	4		
DMF-CO_2-III	**DCMD**	Desalination of 35 g/L NaCl	5.93	11.25	3	3.07	(73.14
		Desalination of 35 g/L $NaNO_3$	±1.11	7.90	3	±0.21	±4.09)*
		Desalination of 450 ppm		6.01	6		
	AGMD	(Cs, Cr and Co) + 35 g/L $NaNO_3$	—	12.76	4		

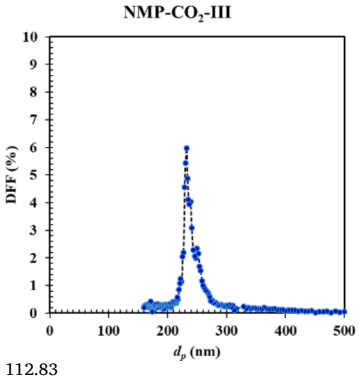

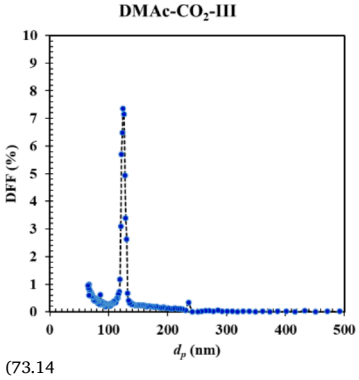

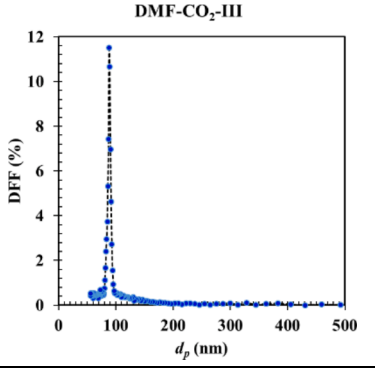

(*) The DMF-CO_2-III membrane's average pore size r_m (m) was obtained using the Guerout-Elford-Ferry equation [64,65]: $r_m = \sqrt{\frac{(2.9-1.75\varepsilon)\times 8\mu\delta Q_t}{\varepsilon \times A \times \Delta P}}$; where, η was the water viscosity at 25 °C, δ was the membrane thickness (m), Q_t was the volume of the permeate water per unit time (m^3/h), A was the effective area of the membrane (m^2), and ΔP was the operational pressure (0.1 MPa).

higher CO_2 concentrations made the coagulant weaker and increased the thermodynamic stability of the casting solution. Consequently, solvent/nonsolvent transport during membrane formation becomes slower as the CO_2 concentration in the coagulation bath increases. This makes demixing slow enough to form a uniform, narrower finger-like structure in which the intermediate voids are eliminated, particularly when using high concentrations of PVDF (15 wt%). This is consistent with the observed trends in the solubility of CO_2 in the studied solvents (see Fig. 2 and Table S1). Consequently, a larger amount of nonsolvent is required to induce phase separation at higher CO_2 concentrations. The amount of water needed to induce the phase change will always be less than that needed for the PVDF/DMF system, however, because of the greater solubility of CO_2 in NMP. As in the case of the DMF systems, the thermodynamic stability of the PVDF/NMP/nonsolvent systems increased with the concentration of CO_2 in the coagulation bath, indicating that water is a strong nonsolvent for the PVDF/NMP system but becomes a

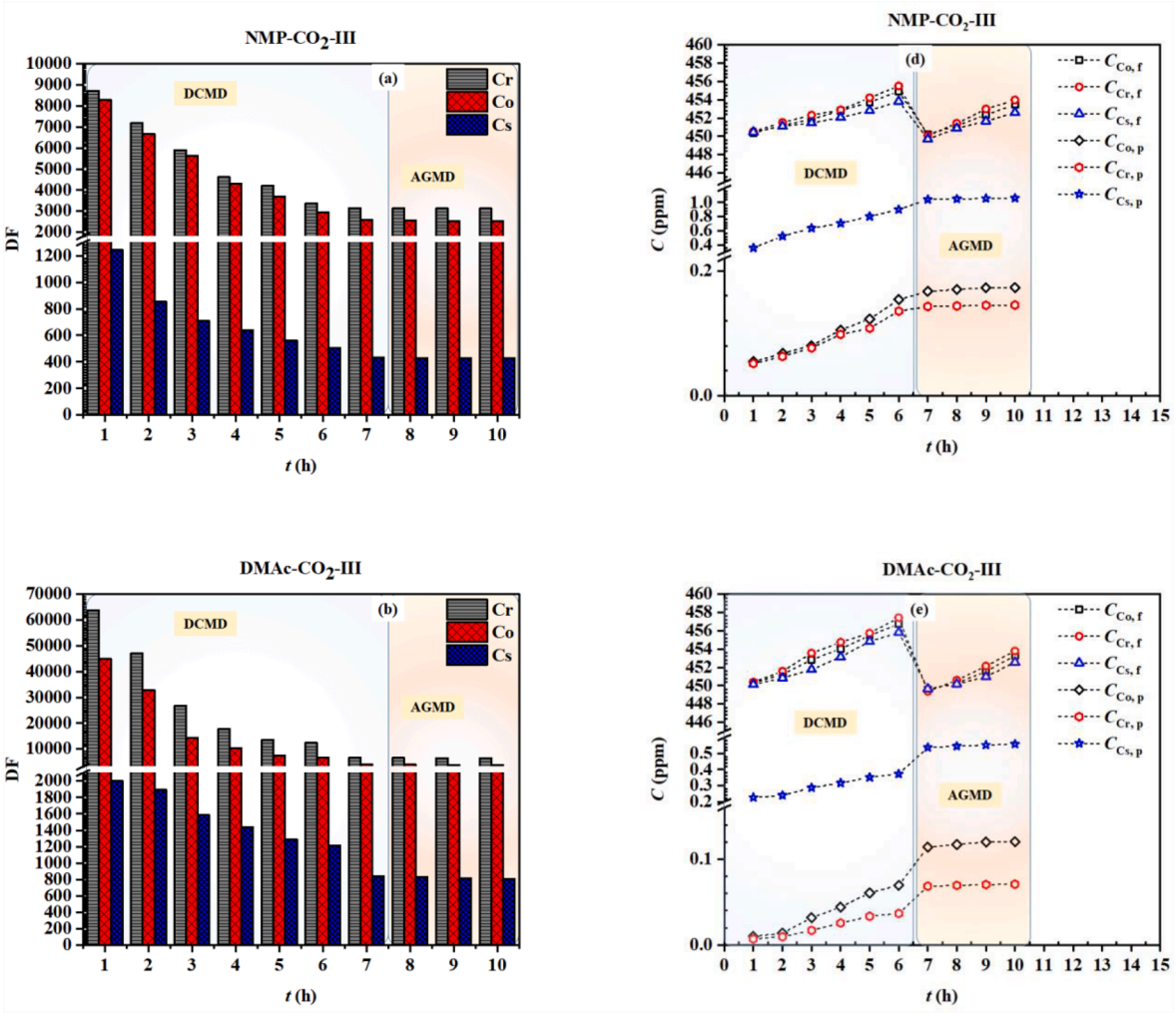

Fig. 12. DCMD and AGMD performances of PVDF membranes expressed in terms of the *DF* (a: NMP, b: DMAc, c: DMF) and the measured nuclide concentration in the permeate (d: NMP, e: DMAc, f: DMF). Also shown are the *DFs* achieved with each membrane (expressed in %) during DCMD (g) and AGMD (h).

progressively weaker nonsolvent as its content of dissolved CO_2 increases.

SEM images showed that all membranes formed in the PVDF/DMAc/water systems had an asymmetric structure with a top skin layer, a finger-like layer, and an underlying sponge-like layer. As shown in Fig. 6, adding CO_2 to the coagulation bath increased its nonsolvent power due to the high solubility of CO_2 in DMAc (compared to that in DMF). This means that a relatively small amount of nonsolvent is needed to induce phase inversion, especially when using the highest CO_2 concentration in the coagulation bath (Level III). When using 10 wt% PVDF casting solutions in DMAc, the finger-like macrovoids became longer as the CO_2 concentration in the coagulation bath increased: the ratio of their length to their thickness increased from 42.1% for distilled water to 63.0% for carbonated water with the highest CO_2 concentration (level III). Similarly, for membranes prepared with a 15 wt% PVDF casting solution, the length ratios of the finger-like macro voids rose from 35% for distilled water to 55% for the level III CO_2 coagulant bath. This is because adding CO_2 to the bath causes more severe disturbance of the solution system's equilibrium (Fig. 6). Accordingly, the turbidity curve of the PVDF/DMAc system shifts towards the nonsolvent polymer axis as the CO_2 concentration increases, indicating a widening of the demixing gap and a reduction in the tolerance of the nonsolvent. In other words, carbonated water is a much stronger nonsolvent than distilled water for the PVDF/DMAc system.

Consequently, the diffusion kinetics of carbonated water in the membrane are faster than those of distilled water, and phase inversion occurs more rapidly for the PVDF/DMAc system when using a carbonated coagulation bath, especially when using high CO_2 levels and low PVDF concentrations. The thermodynamic stability of the PVDF/DMAc/nonsolvent systems thus decreases as the CO_2 content decreases, and water with a high content of CO_2 is a strong nonsolvent for the PVDF/DMAc system.

3.3. Physical properties of membranes

Membrane porosity correlates strongly with the overall membrane microstructure and directly affects the membrane's permeability and tensile strength. Fig. 7 shows the PWP and ε for the fabricated membranes. In general, the ε decreases as the PVDF concentration increases, independently of the solvent type or the nature of the external coagulant (Fig. 7b, d, and f). The variation in the PWP across PVDF membranes prepared with various solvents and precipitated in distilled water with different levels of CO_2 is shown in Fig. 7a, c, and e. The PWP values for membranes prepared from 10 wt% PVDF solutions in NMP, DMAc, and

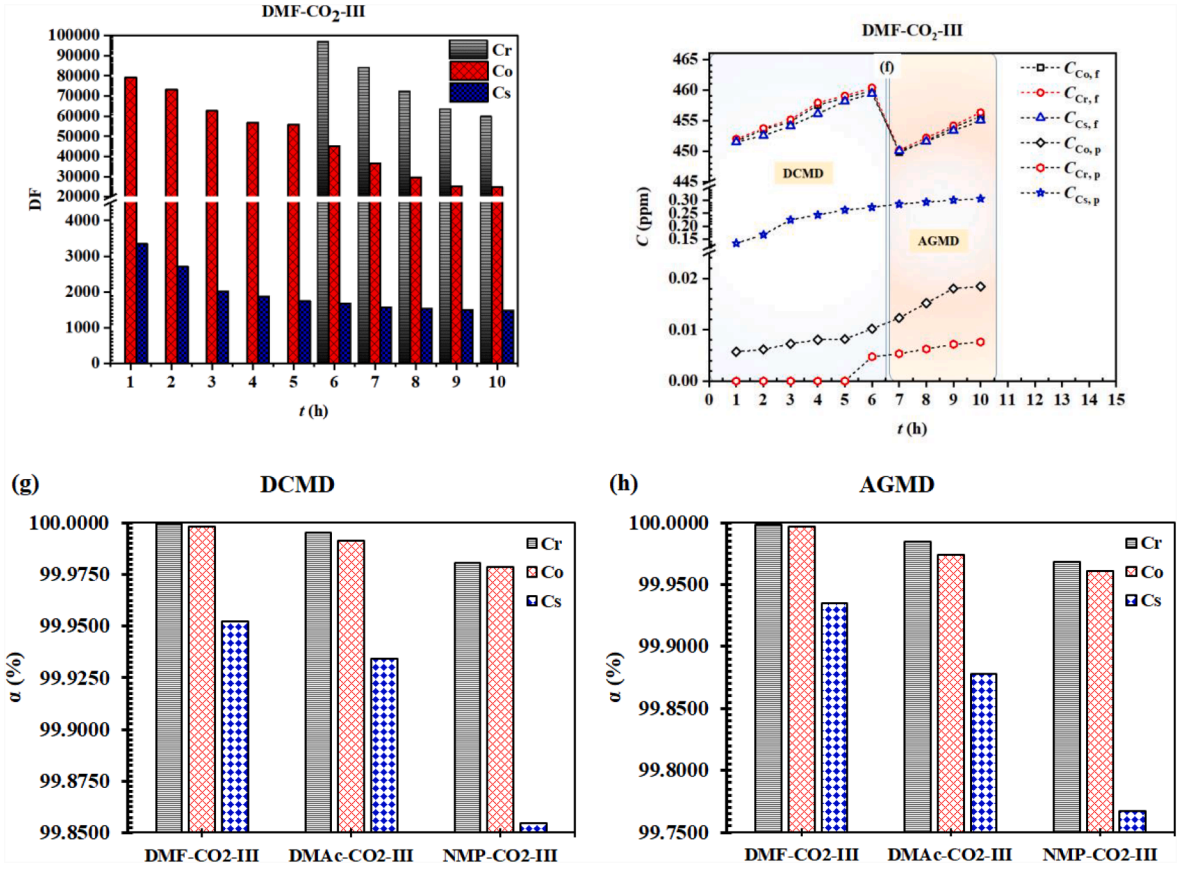

Fig. 12. (*continued*).

DMF using a distilled water coagulation bath were 473.3, 141.3, and 11.1 $L{\cdot}m^{-2}{\cdot}h^{-1}$, respectively. Going from the distilled water coagulation bath to the highest tested CO_2 concentration increased these values to 584.7, 210.7, and 2.8 $L{\cdot}m^{-2}{\cdot}h^{-1}$, respectively. Thus in both cases, the highest ε was achieved using NMP as the solvent, followed by DMAc and then DMF, in accordance with the cross-sectional SEM images (Figs. 3-6) of the membranes.

Fig. 8 shows that the average pore size of the prepared membranes varied widely between the three solvent/PVDF systems; membranes prepared using PVDF/NMP had larger pores than those prepared using PVDF/DMAC and PVDF/DMF. In addition, the pore size decreased slightly as the concentration of the polymer solution increased. These trends are consistent with the variation in the PWP fluxes and porosities of the membranes (Fig. 7), and the cross-sectional SEM images of the membranes shown in Figs. 3-6.

The stress–strain properties of the fabricated microporous PVDF membranes are shown in Fig. 9. The dependence of the membrane's mechanical properties on the polymer concentration in the casting solution is well known; in general, increasing the concentration of the polymer improves the mechanical properties of the resulting membrane. This is because, regardless of the solvent type or the CO_2 content of the external coagulant, ε decreases as the PVDF concentration increases. Moreover, increasing the carbonation of the coagulation bath delayed demixing during the phase inversion process, leading to the formation of a densely microstructured upper layer and a sponge-like microstructure with suppression of macrovoid formation in the bottom layer, especially for the PVDF/DMF system. This reduced the ε percentage and improved the membranes' tensile strengths.

In general, the physical properties of the membranes fabricated in this work are suitable for microfiltration applications; their mean pore sizes range from 0.114 to 1.280 μm and their ε is between 43.1 and 75.2%. The membranes with the highest PWP values (NMP-CO_2-III, DMAc-CO_2-III, and DMF-CO_2-III) were selected for testing in MD experiments. Therefore, these membranes were dried at ambient temperature for 48 h, after which their average pore size, pore size distribution, and LEP_w were measured.

3.4. Polymorphism of prepared membranes

To investigate the crystalline phase of the fabricated PVDF membranes, they were characterized by FTIR spectroscopy. PVDF is known to crystallize into five different polymorphs that are characterized by different conformations of the polymeric backbone: α (phase II), β (phase I), γ (phase III), δ, and ε. The α, β, and/or γ phases are commonly formed during membrane fabrication, and each of them has distinct performance characteristics [59,60]. FTIR spectra of the membranes fabricated in this work are shown in Fig. 10. The 510 and 840 cm^{-1} bands [61,62] characteristic of the β-phase are clearly visible in all of the spectra, together with the bands at 490, 530, 613, 763, 795, 975 cm^{-1} that are associated with α-phase [63]. Both the α- and β-phases are thus present in all of the membranes, indicating that the composition of the coagulation medium had little effect on their polymorphism.

3.5. Desalination and removal of nuclides by MD

Fig. 11 shows the J_p values obtained for distilled feed water, aqueous salt solutions (35 g/L NaCl and 35 g/L $NaNO_3$), and aqueous salt solutions containing non-radioactive metal ions (450 ppm of Cs^+, Cr^{3+}, or Co^{2+} with 35 g/L of $NaNO_3$) during MD experiments using the NMP-CO_2-III, DMAc-CO_2-III, and DMF-CO_2-III membranes, as well as the

Table 3
Atomic percentages of chromium (Cr), cobalt (Co), cesium (Cs), fluorine (F), and carbon (C) determined by EDX analysis.

Membrane	Nuclides				
	Cr	Co	Cs	F	C
NMP--CO_2-III	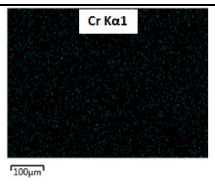	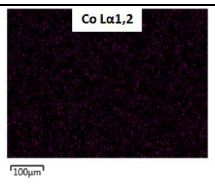	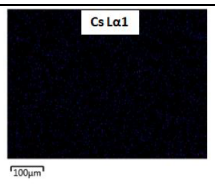	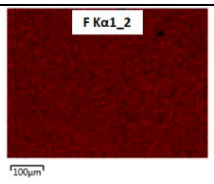	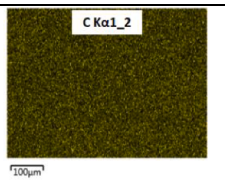
wt%	2.4	0.7	0.2	58.6	38.1
DMAc-CO_2-III	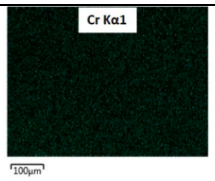	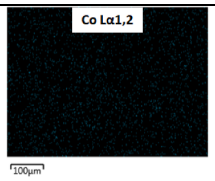	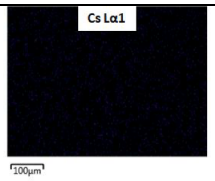	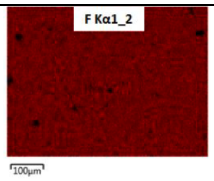	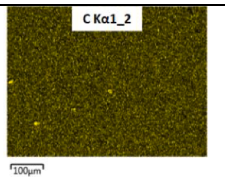
wt%	2.8	1.0	0.3	58.3	37.6
DMF-CO_2-III	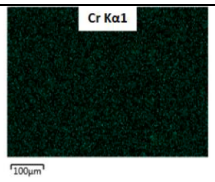	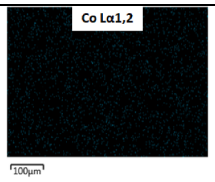	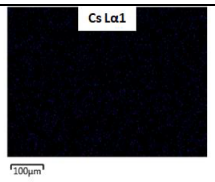	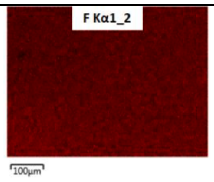	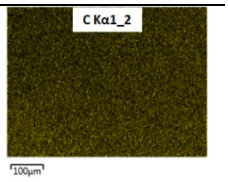
wt%	3.1	1.5	0.4	58.5	36.5

variation in the electrical conductivity of the resulting permeates. The NMP-CO_2-III membrane had the highest J_p value (Fig. 11a), which was attributed to its high ε (75.2%); both the DMAc-CO_2-III (72.0%) and DMF-CO_2-III (54.7%) membranes were appreciably less porous. The high J_p of the NMP-CO_2-III membrane is also partly due to its cross-sectional structure, and specifically its macrovoid-containing sponge-like bottom layer (see Fig. 5). The presence of salts in the feed solution during the MD experiments slightly reduced the J_p because it reduced the water vapor pressure of the feed solution.

The salt (NaCl and $NaNO_3$) rejection factors of all three tested membranes were above 99.5%, regardless of the MD configuration and the type of salt (see Fig. 11a). In addition to achieving higher permeate fluxes than the other two membranes, NMP-CO_2-III membrane also exhibited the greatest increase in the electrical conductivity of the permeate in the DCMD/AGMD experiments, as shown in Table 2. This was due to its low LEP_w value and large pore sizes when compared to the DMAc-CO_2-III, and DMF-CO_2-III membranes (Table 2).

The stable performance of the DMF-CO_2-III membrane in terms of permeate electrical conductivity, salt rejection, and nuclide decontamination during DCMD/AGMD was attributed to its high LEP_w values and low mean pore size (Table 2). In addition, the electrical conductivity of the DMF-CO_2-III permeate remained almost constant during all desalination processes using the DCMD and AGMD configurations, and its *DFs* were higher than those for the other tested membranes (Fig. 11b).

Fig. 12 shows the DF and α for the NMP-CO_2-III, DMAc-CO_2-III, and DMF-CO_2-III membranes during SNWW MD. For NMP-CO_2-III (Fig. 12a and b), DCMD reduced the nuclide content from around 450 ppm in the feed solution to 0.66 ppm in the permeate in the case of Cs^+, 0.09 ppm for Cr^{3+}, and 0.10 ppm for Co^{2+}, giving *DFs* above 752, 5667, and 5255, respectively. In AGMD, the nuclide concentration was reduced from around 450 ppm to 1.05 ppm for Cs^+, 0.14 ppm for Cr^{3+}, and 0.18 ppm for Co^{2+}, giving decontamination factors of 429, 3135, and 2548, respectively.

More remarkably, the DMF-CO_2-III membrane (Fig. 12c and f) achieved extremely high *DFs* of 2228 for Cs^+, ∞ for Cr^{3+} (if presence the concentration is less than the detection limit of the instrument), and 62,102 for Co^{2+} in DCMD experiments. The corresponding *DFs* for the AGMD configuration were 1529, 69839, and 29036, respectively.

Over 10-hour operating periods, the nuclide removal efficiencies achieved using DCMD and AGMD (expressed as percentages) were in excess of 99.85% and 99.75%, respectively (Fig. 12g and h), especially when using the DMF-CO_2-III membrane. This indicates that DCMD and/or AGMD using flat membranes coagulated in carbonated water could be an efficient method for removing radionuclides from saline nuclear wastewater solutions.

To further evaluate the stability and degree of fouling of the membranes tested during the MD experiments, energy dispersive X-ray spectroscopy (EDX- X-Max, OXFORD Instruments) experiments were performed to determine the abundance of Co, Cr, and Cs on the surface of membrane samples after removal from the MD module. EDX analysis was used to map an area of about 600 × 450 μm on the membrane surface, as shown in Table 3. The atomic percentages of chromium (Cr), cobalt (Co), cesium (Cs), fluorine (F), and carbon (C) together with the ratio of the atomic percentages of each nuclide to the sum of fluorine and carbon (F + C) are shown for each membrane in Fig. 13. It is clear that the DMF-CO_2-III membrane has the highest atomic percentages of each nuclide and the highest (nuclide/F + C) ratios. These results are

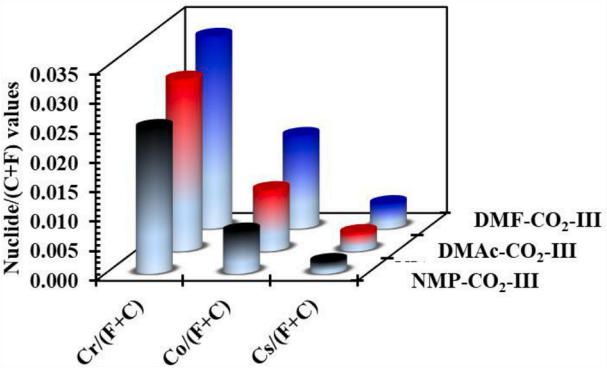

Fig 13. The ratio of the atomic percentages of each nuclide to the sum of fluorine and carbon (F + C) determined by EDX analysis.

Table 4
Performance of previously reported membranes in wastewater treatment using MD.

MD type-membrane material	Feed content		α (%)	DF	J_p ($L{\cdot}m^{-2}{\cdot}h^{-1}$)	Conditions	Ref
	Nuclides	Salt					
VMD-PP	Sr (II) at 10 mg/LCo (II) at 11 mg/L	—	99.60–99.74 99.67–99.82	– 	6.71 6.30	T_f: 70 °C P_v: 0.98 atm	[66]
DCMD-PES & PS with SMMs	60Co – 1 mS/cm 137Cs – 1 mS/cm 85Sr – 1 mS/cm	—	99.69–99.93	400 – 1000 900 – 1400 400–800	0.06–0.16	T_f: 55 °C T_p: 21.5 °C	[41]
DCMD-PP	Co (II), Sr (II) and Cs (I) at 100 mg/L	$NaNO_3$ at (0–300 g/L)	—	10^5 –10^6	19.5 – 15.8	T_f: 70 °C T_p: 20 °C	[40]
VMD-PP	Cs(II) at 100 mg/LCo(II) at 100 mg/LSr(II) at 100 mg/L	80 g/L	98.66 99.03 97.83	6000 3700 8300	5.4	T_f: 75 P_v: 4 kPa	[67]
VMD- PTFE	Cs (II) at 20 mg/L	—	—	$10^{4.85}$	6.82	T_f: 90 P_v: 10 kPa	[42]
DCMD-NMP-CO_2-III	Cr(III) at 450 ppmCo(II) at 450 ppmCs(II) at 450 ppm	35 g/L $NaNO_3$	99.9804 99.9785 99.8548	5667 5255 752	19.70	T_f: 70 °C T_p: 20 °C	This study
DCMD-DMAc-CO_2-III	Cr(II) at 450 ppmCo(II) at 450 ppmCs(II) at 450 ppm		99.9953 99.9916 99.9341	30,194 19,388 1571	15.46		
DCMD-DMF-CO_2-III	Cr(II) at 450 ppmCo(II) at 450 ppmCs(II) at 450 ppm		99,9998 99.9983 99.9522	96,815 62,102 2228	11.24		
AGMD-NMP-CO_2-III	Cr(II) at 450 ppmCo(II) at 450 ppmCs(II) at 450 ppm		99.9681 99.9785 99.8548	3135 5255 752	13.38	T_f: 70 °C T_c: 20 °C	
AGMD-DMAc-CO_2-III	Cr(II) at 450 ppmCo(II) at 450 ppmCs(II) at 450 ppm		99.9845 99.9739 99.8783	6497 3846 826	10.08		
AGMD-DMF-CO_2-III	Cr(II) at 450 ppmCo(II) at 450 ppmCs(II) at 450 ppm		99.9985 99.9965 99.9346	69,839 29,036 1529	7.51		

(*) VMD, vacuum membrane distillation; PP, polypropylene; DCMD, direct contact membrane distillation; PES, polyethersulfone; PS, Polysulfone; FO, forward osmosis; CTA-ES, Cellulose triacetate with embedded polyester screen support; RWW, Radioactive wastewater; PTFE, Polytetrafluoroethylene;

consistent with the degrees of decontamination recorded during the MD assays, which were higher for the DMF-CO_2-III membrane than for the DMAc-CO_2-III and NMP-CO_2-III membranes (see Figs. 11 and 12).

After performing the MD experiments, the J_p through the membranes was again measured using distilled water as the feed solution to determine whether there had been any change in the membranes' performance. No significant reduction in J_p was observed; the observed reductions were between 3% and 8%, indicating only modest fouling. For comparative purposes, Table 4 shows the results obtained with some previously reported PVDF planar membranes developed for MD and used in SNWW desalination and decontamination experiments. When compared to these previously reported membranes, the membranes examined in this work exhibit good desalination stability with high permeate fluxes, α, and *DFs*.

4. Conclusions

Carbon dioxide (CO_2) dissolved in water was used as a coagulation medium to produce porous PVDF membranes. The effects of three different solvents for membrane preparation, namely DMF, DMAc, and NMP, and the CO_2 concentration in the coagulation bath were investigated. It was found that adding CO_2 to the coagulation bath led to the formation of membranes with asymmetric structures and pore sizes suitable for MD, especially when using a low concentration of PVDF (10 wt%). Increasing the CO_2 content in the coagulation bath to a maximum of 0.80 g/L caused a gradual change in membrane structure and altered the demixing kinetics during the phase inversion process, leading to changes in the *PWP* and the performance of both DCMD, and AGMD configurations of the fabricated membranes.

When tested in DCMD and AGMD processes, the fabricated membranes efficiently rejected Cs^+, Co^{2+}, and Cr^{3+} in simulated wastewater. Particularly good performance was achieved with the DMF-CO_2-III membrane. During continuous DCMD operation, the *DFs* for Cr, Co, and Cs reached values of 62×10^3, 96×10^3, and 22×10^2, respectively, with a α>99.99% when using a feed solution containing 450 ppm of each nuclide and 35 g/L $NaNO_3$. Moreover, the permeate flow rate could be maintained at 11.24 $kg.m^{-2}h^{-1}$ while restricting the electrical conductivity of the permeate to only ~ 6.01 μS/cm. Using the same feed solution in the AGMD configuration, the *DFs* for Cr, Co, and Cs were 26×10^3, 69×10^3, and 15×10^2, respectively, with a α of 99.99%. The permeate flow rate in this case was maintained at 7.51 $kg.m^{-2}h^{-1}$ with an electrical conductivity of ~ 12.76 μS/cm.

In addition to their favorable performance, the fabricated membranes exhibited no strong tendency towards pore contamination due to adsorption of radioactive elements and allowed efficient single-step decontamination of simulated nuclear wastewater. Given that nuclear wastewater treatment is most often needed in environments where waste heat is readily available such as nuclear power plants, MD is clearly an attractive option. However, more research is needed to test the feasibility of the fabricated membranes in real nuclear wastewater treatment. The results presented herein show that by using CO_2 dissolved in distilled water as a non-toxic coagulation medium it is possible to prepare PVDF membranes with diverse structures and potential applications in MD. Importantly, the structural features of the obtained membranes can be tuned by varying the concentration of the PVDF solution, the choice of solvent, and the level of CO_2 in the coagulation bath. As such, these results demonstrate that CO_2 is a viable and environmentally friendly nonsolvent additive for polymeric membrane fabrication with important advantages in terms of morphological control of the fabricated membranes.

Declaration of Competing Interest

The authors declare that they have no known competing financial interests or personal relationships that could have appeared to influence the work reported in this paper.

Acknowledgments

The Bio4Energy programme (B4E3-TM-2) and Kempe Foundations (JCK22-0008) are gratefully acknowledged. The authors would like to express their appreciation for the financial support of the National Natural Science Foundation of China (22078146), Natural Science Foundation of Jiangsu Province (BK20200091). This work is a part of activities of the Technical Chemistry, Department of Chemistry, Chemical-Biological Centre, Umeå University, Sweden as well as the Johan Gadolin Process Chemistry Centre at Åbo Akademi University in Finland.

Appendix A. Supplementary data

Supplementary data to this article can be found online at https://doi.org/10.1016/j.cej.2022.137300.

References

[1] M.K. Purkait, R. Singh, Membrane technology in separation science, CRC Press, 2018.
[2] M. Mulder, Membrane preparation | phase inversion membranes, in: I.D. Wilson (Ed.), Encyclopedia of Separation Science, Academic Press, Oxford, 2000, pp. 3331–3346.
[3] D.-M. Wang, A. Venault, J.-Y. Lai, Chapter 2 - Fundamentals of nonsolvent-induced phase separation, in: T.-S. Chung, Y. Feng (Eds.) Hollow Fiber Membranes, Elsevier2021, pp. 13-56.
[4] M. Mulder, Preparation of synthetic membranes, Springer, Netherlands, Dordrecht, Basic Principles of Membrane Technology, 1996, pp. 71–156.
[5] S. Fadhil, T. Marino, H.F. Makki, Q.F. Alsalhy, S. Blefari, F. Macedonio, E.D. Nicolò, L. Giorno, E. Drioli, A. Figoli, Novel PVDF-HFP flat sheet membranes prepared by triethyl phosphate (TEP) solvent for direct contact membrane distillation, Chem. Eng. Process. Process Intensif. 102 (2016) 16–26.
[6] I.S. Makarov, L.K. Golova, M.I. Vinogradov, M.V. Mironova, T.S. Anokhina, N. A. Arkharova, Morphology and transport properties of membranes obtained by coagulation of cellulose solutions in isobutanol, Carbohydr. Polym. 254 (2021), 117472.
[7] P. Sukitpaneenit, T.-S. Chung, Molecular elucidation of morphology and mechanical properties of PVDF hollow fiber membranes from aspects of phase inversion, crystallization and rheology, J. Membr. Sci. 340 (2009) 192–205.
[8] D.-Y. Zuo, B.-K. Zhu, J.-H. Cao, Y.-Y. Xu, Influence of alcohol-based nonsolvents on the formation and morphology of PVDF membranes in phase inversion process, Chin. J. Polym. Sci. 24 (2006) 281–289.
[9] S. Munirasu, F. Banat, A.A. Durrani, M.A. Haija, Intrinsically superhydrophobic PVDF membrane by phase inversion for membrane distillation, Desalination 417 (2017) 77–86.
[10] M.G. Buonomenna, P. Macchi, M. Davoli, E. Drioli, Poly(vinylidene fluoride) membranes by phase inversion: the role the casting and coagulation conditions play in their morphology, crystalline structure and properties, Eur. Polym. J. 43 (2007) 1557–1572.
[11] G.J. Dahe, R.P. Singh, K.W. Dudeck, D. Yang, K.A. Berchtold, Influence of non-solvent chemistry on polybenzimidazole hollow fiber membrane preparation, J. Membr. Sci. 577 (2019) 91–103.
[12] J. Chang, J. Zuo, L. Zhang, G.S. O'Brien, T.-S. Chung, Using green solvent, triethyl phosphate (TEP), to fabricate highly porous PVDF hollow fiber membranes for membrane distillation, J. Membr. Sci. 539 (2017) 295–304.
[13] S. Nejati, C. Boo, C.O. Osuji, M. Elimelech, Engineering flat sheet microporous PVDF films for membrane distillation, J. Membr. Sci. 492 (2015) 355–363.
[14] T.-H. Young, L.-P. Cheng, D.-J. Lin, L. Fane, W.-Y. Chuang, Mechanisms of PVDF membrane formation by immersion-precipitation in soft (1-octanol) and harsh (water) nonsolvents, Polymer 40 (1999) 5315–5323.
[15] Z. Liu, J. Xiang, X. Hu, P. Cheng, L. Zhang, W. Du, S. Wang, N. Tang, Effects of coagulation-bath conditions on polyphenylsulfone ultrafiltration membranes, Chin. J. Chem. Eng. (2021).
[16] S. Mazinani, S. Darvishmanesh, A. Ehsanzadeh, B. Van der Bruggen, Phase separation analysis of Extem/solvent/non-solvent systems and relation with membrane morphology, J. Membr. Sci. 526 (2017) 301–314.
[17] K.-Y. Chun, S.-H. Jang, H.-S. Kim, Y.-W. Kim, H.-S. Han, Y.-I. Joe, Effects of solvent on the pore formation in asymmetric 6FDA–4,4′ODA polyimide membrane: terms of thermodynamics, precipitation kinetics, and physical factors, J. Membr. Sci. 169 (2000) 197–214.
[18] M.A. Yam-Cervantes, J.L. Santiago-García, M.I. Loría-Bastarrachea, S. Duarte-Aranda, F. Alberto Ruiz-Treviño, M. Aguilar-Vega, Sulfonated polyphenylsulfone asymmetric membranes: Effect of coagulation bath (acetic acid-NaHCO3/isopropanol) on morphology and antifouling properties, Journal of Applied Polymer Science 134 (2017).
[19] J.Y. Kim, H.K. Lee, S.C. Kim, Liquid-liquid phase separation during polysulfone membrane preparation, Korean J. Chem. Eng. 17 (2000) 564–569.
[20] L.-P. Cheng, T.-H. Young, W.-M. You, Formation of crystalline EVAL membranes by controlled mass transfer process in water–DMSO–EVAL copolymer systems, J. Membr. Sci. 145 (1998) 77–90.
[21] C.-Y. Kuo, H.-N. Lin, H.-A. Tsai, D.-M. Wang, J.-Y. Lai, Fabrication of a high hydrophobic PVDF membrane via nonsolvent induced phase separation, Desalination 233 (2008) 40–47.
[22] M.A. Silva, E. Belmonte-Reche, M.T.P. de Amorim, Morphology and water flux of produced cellulose acetate membranes reinforced by the design of experiments (DOE), Carbohydr. Polym. 254 (2021), 117407.
[23] L.-P. Cheng, T.-H. Young, L. Fang, J.-J. Gau, Formation of particulate microporous poly(vinylidene fluoride) membranes by isothermal immersion precipitation from the 1-octanol/dimethylformamide/poly(vinylidene fluoride) system, Polymer 40 (1999) 2395–2403.
[24] Q. Li, Z.-L. Xu, M. Liu, Preparation and characterization of PVDF microporous membrane with highly hydrophobic surface, Polym. Adv. Technol. 22 (2011) 520–531.
[25] M. Pagliero, A. Bottino, A. Comite, C. Costa, Novel hydrophobic PVDF membranes prepared by nonsolvent induced phase separation for membrane distillation, J. Membr. Sci. 596 (2020), 117575.
[26] J.T. Jung, J.F. Kim, H.H. Wang, E. di Nicolo, E. Drioli, Y.M. Lee, Understanding the non-solvent induced phase separation (NIPS) effect during the fabrication of microporous PVDF membranes via thermally induced phase separation (TIPS), J. Membr. Sci. 514 (2016) 250–263.
[27] M. Iqbal, Z. Man, H. Mukhtar, B.K. Dutta, Solvent effect on morphology and CO2/CH4 separation performance of asymmetric polycarbonate membranes, J. Membr. Sci. 318 (2008) 167–175.
[28] D.-J. Lin, C.-L. Chang, T.-C. Chen, L.-P. Cheng, Microporous PVDF membrane formation by immersion precipitation from water/TEP/PVDF system, Desalination 145 (2002) 25–29.
[29] X. Yang, S.R. Liew, R. Bai, Simultaneous alkaline hydrolysis and non-solvent induced phase separation method for polyacrylonitrile (PAN) membrane with highly hydrophilic and enhanced anti-fouling performance, J. Membr. Sci. 635 (2021), 119499.
[30] H. Wang, T. Wang, S. Yang, L. Fan, Preparation of thermal stable porous polyimide membranes by phase inversion process for lithium-ion battery, Polymer 54 (2013) 6339–6348.
[31] W.Y. Chuang, T.H. Young, W.Y. Chiu, C.Y. Lin, The effect of polymeric additives on the structure and permeability of poly(vinyl alcohol) asymmetric membranes, Polymer 41 (2000) 5633–5641.
[32] M.H. Razzaghi, M. Tavakolmoghadam, F. Rekabdar, F. Oveisi, Investigation of the effect of coagulation bath composition on PVDF/CA membrane by evaluating critical flux and antifouling properties in lab-scale submerged MBR, Water and Environment Journal 32 (2018) 366–376.
[33] C.Y. Lai, A. Groth, S. Gray, M. Duke, Impact of casting conditions on PVDF/nanoclay nanocomposite membrane properties, Chem. Eng. J. 267 (2015) 73–85.
[34] D.M. Koenhen, M.H.V. Mulder, C.A. Smolders, Phase separation phenomena during the formation of asymmetric membranes, J. Appl. Polym. Sci. 21 (1977) 199–215.
[35] D.-J. Lin, C.-L. Chang, C.-K. Lee, L.-P. Cheng, Preparation and characterization of microporous PVDF/PMMA composite membranes by phase inversion in water/DMSO solutions, Eur. Polym. J. 42 (2006) 2407–2418.
[36] J.G. Wijmans, J.P.B. Baaij, C.A. Smolders, The mechanism of formation of microporous or skinned membranes produced by immersion precipitation, J. Membr. Sci. 14 (1983) 263–274.
[37] I.A.E. Agency, Technologies for Remediation of Radioactively Contaminated Sites, International Atomic Energy Agency (1999).
[38] IAEA, Improvements of Radioactive Waste Management at WWER Nuclear Power Plants, IAEA Vienna, 2006.
[39] G. Zakrzewska-Trznadel, M. Harasimowicz, A.G. Chmielewski, Membrane processes in nuclear technology-application for liquid radioactive waste treatment, Sep. Purif. Technol. 22 (2001) 617–625.
[40] X. Wen, F. Li, X. Zhao, Removal of nuclides and boron from highly saline radioactive wastewater by direct contact membrane distillation, Desalination 394 (2016) 101–107.
[41] M. Khayet, Treatment of radioactive wastewater solutions by direct contact membrane distillation using surface modified membranes, Desalination 321 (2013) 60–66.
[42] X. Jia, L. Lan, X. Zhang, T. Wang, Y. Wang, C. Ye, J. Lin, Pilot-scale vacuum membrane distillation for decontamination of simulated radioactive wastewater: System design and performance evaluation, Sep. Purif. Technol. 275 (2021), 119129.
[43] X. Nie, X. Hu, C. Liu, X. Xia, F. Dong, Decontamination of uranium contained low-level radioactive wastewater from UO2 fuel element industry with vacuum membrane distillation, Desalination 516 (2021), 115226.
[44] Y.I. Dytnerskii, Y.V. Karlin, B. Kropotov, Prospects for using membrane distallation for reprocessing liquid radioactive wastes, Atomic Energy (New York) 75 (1994).
[45] G. Zakrzewska-Trznadel, M. Harasimowicz, A.G. Chmielewski, Concentration of radioactive components in liquid low-level radioactive waste by membrane distillation, J. Membr. Sci. 163 (1999) 257–264.

[46] R.H. Weiland, O. Trass, Titrimetric determination of acid gases in alkali hydroxides and amines, Anal. Chem. 41 (1969) 1709–1710.
[47] T.G. Amundsen, L.E. Øi, D.A. Eimer, Density and Viscosity of Monoethanolamine + Water + Carbon Dioxide from (25 to 80) °C, J. Chem. Eng. Data 54 (2009) 3096–3100.
[48] R.M. Boom, T. van den Boomgaard, J.W.A. van den Berg, C.A. Smolders, Linearized cloudpoint curve correlation for ternary systems consisting of one polymer, one solvent and one non-solvent, Polymer 34 (1993) 2348–2356.
[49] A. Okubo, Diffusion: Mass Transfer in Fluid Systems, University of Chicago Press, 1987.
[50] C.M. Hansen, Hansen Solubility Parameters (1967) 104–117.
[51] A. Bottino, G. Camera-Roda, G. Capannelli, S. Munari, The formation of microporous polyvinylidene difluoride membranes by phase separation, J. Membr. Sci. 57 (1991) 1–20.
[52] M. Essalhi, M. Khayet, S. Tesfalidet, M. Alsultan, N. Tavajohi, Desalination by direct contact membrane distillation using mixed matrix electrospun nanofibrous membranes with carbon-based nanofillers: A strategic improvement, Chem. Eng. J. 426 (2021), 131316.
[53] M. Essalhi, M. Khayet, Surface segregation of fluorinated modifying macromolecule for hydrophobic/hydrophilic membrane preparation and application in air gap and direct contact membrane distillation, J. Membr. Sci. 417–418 (2012) 163–173.
[54] J. Li, D. Xu, W. Wang, X. Wang, Y. Mao, C. Zhang, W. Jiang, C. Wu, Review on Selection and Experiment Method of Commonly Studied Simulated Radionuclides in Researches of Nuclear Waste Solidification, Science and Technology of Nuclear Installations 2020 (2020) 3287320.
[55] M. Khayet, J. Mengual, G. Zakrzewska-Trznadel, Direct contact membrane distillation for nuclear desalination, Part II: experiments with radioactive solutions, International journal of nuclear desalination 2 (2006) 56–73.
[56] X. Wen, F. Li, B. Jiang, X. Zhang, X. Zhao, Effect of surfactants on the treatment of radioactive laundry wastewater by direct contact membrane distillation, J. Chem. Technol. Biotechnol. 93 (2018) 2252–2261.
[57] C.J. Davey, P. Liu, F. Kamranvand, L. Williams, Y. Jiang, A. Parker, S. Tyrrel, E. J. McAdam, Membrane distillation for concentrated blackwater: Influence of configuration (air gap, direct contact, vacuum) on selectivity and water productivity, Sep. Purif. Technol. 263 (2021), 118390.
[58] F. Liu, N.A. Hashim, Y. Liu, M.R.M. Abed, K. Li, Progress in the production and modification of PVDF membranes, J. Membr. Sci. 375 (2011) 1–27.
[59] T. Boccaccio, A. Bottino, G. Capannelli, P. Piaggio, Characterization of PVDF membranes by vibrational spectroscopy, J. Membr. Sci. 210 (2002) 315–329.
[60] M. Zhang, A.-Q. Zhang, B.-K. Zhu, C.-H. Du, Y.-Y. Xu, Polymorphism in porous poly (vinylidene fluoride) membranes formed via immersion precipitation process, J. Membr. Sci. 319 (2008) 169–175.
[61] J. Gregorio, M. Rinaldo, Cestari, Effect of crystallization temperature on the crystalline phase content and morphology of poly(vinylidene fluoride), J. Polym. Sci., Part B: Polym. Phys. 32 (1994) 859–870.
[62] A. Salimi, A.A. Yousefi, Analysis Method: FTIR studies of β-phase crystal formation in stretched PVDF films, Polym. Test. 22 (2003) 699–704.
[63] T. Nishiyama, T. Sumihara, Y. Sasaki, E. Sato, M. Yamato, H. Horibe, Crystalline structure control of poly(vinylidene fluoride) films with the antisolvent addition method, Polym. J. 48 (2016) 1035–1038.
[64] G.S. Lai, M.H.M. Yusob, W.J. Lau, R.J. Gohari, D. Emadzadeh, A.F. Ismail, P.S. Goh, A.M. Isloor, M.-R.-D. Arzhandi, Novel mixed matrix membranes incorporated with dual-nanofillers for enhanced oil-water separation, Sep. Purif. Technol. 178 (2017) 113–121.
[65] C. Liao, J. Zhao, P. Yu, H. Tong, Y. Luo, Synthesis and characterization of low content of different SiO2 materials composite poly (vinylidene fluoride) ultrafiltration membranes, Desalination 285 (2012) 117–122.
[66] F. Jia, Y. Yin, J. Wang, Removal of cobalt ions from simulated radioactive wastewater by vacuum membrane distillation, Prog. Nucl. Energy 103 (2018) 20–27.
[67] X. Wen, F. Li, X. Zhao, Filtering of Low-Level Radioactive Wastewater by Means of Vacuum Membrane Distillation, Nucl. Technol. 194 (2016) 379–386.